学位論文

Study of the inner-nuclear membrane protein Nemp1 as a binding protein of the nuclear transport regulator Ran GTPase

（核輸送制御因子 Ran GTPase と結合する核内膜蛋白質 Nemp1 に関する研究）

平成２６年９月博士（理学）申請

東京大学大学院理学系研究科

生物科学専攻

柴野　卓志

Contents

Abstract

The inner nuclear membrane (INM) protein Nemp1/TMEM194A has previously been suggested to be involved in eye development in *Xenopus*, and contains two evolutionarily conserved sequences in the transmembrane domains (TMs) and the C-terminal region, named region A and region B, respectively. To elucidate the molecular nature of Nemp1, I analyzed its interacting proteins through those conserved regions. First, I found that Nemp1 interacts with itself and lamin through the TMs and region A, respectively. Colocalization of Nemp1 and lamin at the INM suggests that the interaction with lamin participates in the INM localization of Nemp1. Secondly, through yeast two-hybrid screening using region B as bait, I identified the small GTPase Ran as a probable Nemp1-binding partner. GST pulldown and co-immunoprecipitation assays using region B and Ran mutants revealed that region B binds directly to the GTP-bound Ran through its effector domain. Immunostaining experiments using transfected COS-7 cells revealed that full-length Nemp1 recruits Ran near the nuclear envelope, suggesting a role for Nemp1 in the accumulation of RanGTP at the nuclear periphery. At the neurula-to-tailbud stages of *Xenopus* embryos, *nemp1* expression overlapped with *ran* in several regions including the eye vesicles. Co-knockdown using antisense morpholino oligos for *nemp1* and *ran* caused reduction of cell densities and severe eye defects more strongly than either single knockdown alone, suggesting their functional interaction. Finally I show that *Arabidopsis thaliana* Nemp1-orthologous proteins interact with *A. thaliana* Ran, suggesting their evolutionally conserved physical and functional interactions possibly in basic cellular functions including nuclear transportation. Taken together, I conclude that Nemp1 represents a new type of RanGTP-binding protein.

Abbreviations

BAF, barrier to autointegration factor

BBS, BAF binding site

BSA, bovine serum albumin

Bt, the region B plus its downstream region

co-IP, co-immunoprecipitation

CIAP, calf intestine phosphatase

Ct, the C-terminal region

DAPI, 4',6-diamidino-2-phenylindole

DTT, dithiothreitol

EDTA, ethylenediamine-N,N,N',N'-tetraacetic acid

ER, endoplasmic reticulum

FITC, fluorescein isothiocyanate

GST, glutathione S-transferase

IF, immunofluorescence

INM, inner nuclear membrane

KASH domain, Klarsicht, ANC-1, and Syne-1 homology domain

KR, Lys-Arg-rich

λPP, λ protein phosphatase

LBR, lamin B receptor

MO, morpholino oligo

NE, nuclear envelope

NLS nuclear localization signal

NPC, nuclear pore complex

Nup, nucleoporin

ONM, outer nuclear membrane

PMSF, phenylmethylsulfonyl fluoride

RT-PCR, reverse transcription-polymerase chain reaction

RT-qPCR, reverse transcription-quantitative polymerase chain reaction

SUN domain, Sad and UNC-84 homology domain

SP, signal peptide

TM, transmembrane domain

UTR, untranslated region

WISH, whole-mount *in situ* hybridization

Introduction

Eukaryotes have been considered to emerge from 1.6-2.1 billion years ago through acquiring various organelles, one of which is the nucleus. The nucleus contains DNA that is the molecule carrying the genetic information, and is surrounded by the nuclear envelope (NE). The NE is not only the boundary that separates the nuclear and cytoplasmic compartments of eukaryotic cells, but also plays regulatory roles in chromatin organization and gene expression through its nucleoplasmic surface (Zuleger et al., 2011). The NE is composed of double nuclear membranes, nuclear pore complexes (NPCs), outer nuclear membrane (ONM) proteins, and a fibrous protein meshwork consisting of inner nuclear membrane (INM) proteins and lamins, called the nuclear lamina (Fig. 1). The regulatory role of the NE is mainly attributed to NPCs, lamin, and INM proteins (Wilson and Berk, 2010). Proteome analysis of the NE identified a large number of putative integral NE proteins and its transcriptome profiling exhibited cell-type-specific differences in mammalian cells (Schirmer et al., 2003) implying the possibility that the NE plays some roles in tissue differentiation and development. To examine this possibility, it is important to identify and characterize INM proteins that are tissue-specifically expressed during development.

INM proteins have been shown to bind to lamins and hence reside on the INM (Wilson and Berk, 2010) (Fig. 1). Regarding the function of these INM proteins, lamin B receptor (LBR) is an eight-transmembrane domain protein and interacts with lamin B and heterochromatin protein 1 (HP1) (Fig. 1). LBR plays roles in maintaining nuclear shape and heterochromatin distribution (Olins et al., 2010). SUN domain proteins (Sun1, Sun2, Sun3, and SPAG4 in vertebrates) bind to ONM-localized KASH domain proteins (Nesprin-1, Nesprin-2, Nesprin-3 in vertebrates) through SUN-KASH domain interactions. These complexes associate with actin filaments, microtubules and intermediate filaments to connect the nucleoskeleton and cytoskeleton (Fig. 1). These connections play important roles in nuclear migration and anchoring centrosomes to the nucleus (Razafsky and Hodzic, 2009). LEM domain proteins

(LAP2, Emerin, and MAN1 in vertebrates) interact with barrier to autointegration factor (BAF) through the LEM domain to anchor chromatin to the NE (Fig. 1). Of them, Emerin and MAN1 also bind to signal transducers at the INM to modulate BMP/TGF-β and Wnt signaling. For example, MAN1 binds to R-Smad and attenuates BMP/TGF-β signaling (Osada et al., 2003), and Emerin binds to β-catenin and down-regulates Wnt signaling (Markiewicz et al., 2006) (Fig. 1). Thus, INM proteins play regulatory roles in signal transduction in addition to gene regulation, chromatin organization, and NE formation (Gruenbaum et al., 2005).

NPCs are macromolecular complexes of about 125 MDa embedded in the NE, which are composed of about 30 different nucleoporins (Nups) (Cautain et al., 2015). NPCs mediate the bidirectional transport of proteins and RNAs across the NE. Nuclear transport proteins, such as importin β/karyopherin β, exportin 1/Crm1, and the small GTPase Ran facilitate the transport of proteins through NPCs (Stewart, 2007). Ran exists in a GTP-bound (RanGTP) and a GDP-bound (RanGDP) state, which are enriched in the nucleus and the cytoplasm, respectively (Fig. 2A). Their differential localizations are maintained by RCC1 (the nucleotide exchange factor for Ran), which binds to the chromatin in the nucleus, and by RanGAP1 (the Ran GTPase activating protein) and its cofactors RanBP1 and RanBP2 in the cytoplasm. Importins and exportins function as transporters for various cargos. In the case of nuclear import, cargos are bound by importin β, and transported into the nucleus, then dissociated from importin β in the nucleus upon the binding of importin β to RanGTP through the effector domain of Ran (Fig. 2B). In the case of nuclear export, cargos form a ternary complex with RanGTP and exportin 1 and are transported into the cytoplasm. In the cytoplasm, RanGAP1 attached to the NPC activate the GTPase activity of Ran to convert RanGTP to RanGDP and disassemble the ternary complex to release cargos. Such nuclear transport mechanisms are conserved between animals and plants (Merkle, 2011). Other than nuclear transportation, Ran is also involved in controlling mitotic checkpoints, spindle assembly, and NE re-assembly through its interactions with importins as follows (Clarke and Zhang, 2008; Hughes et al., 1998). From prophase to

metaphase when condensed chromosomes are aligned in the middle of the spindle, RanGTP is concentrated around the chromosome, because chromatin-bound RCC1 converts RanGDP to RanGTP. While importin α/β bind to SAFs (spindle assembly factors) to suppress the activity of SAFs, RanGTP releases SAFs from importin α/β to activate SAFs, resulting in spindle assembly around chromosome (Fig. 3A). In the telophase, the nuclear envelope reassembles around each set of daughter chromosomes by fusing vesicles containing INM proteins. During this time, nucleoporins, such as Nup107, Nup153, Nup358, also translocate near chromatin as an inhibitory complex with importin β, then RanGTP concentrated around chromatin releases the nucleoporins from importin β, allowing assembly of NPCs and vesicle fusion (Fig. 3B). These suggest that Ran is a crucial factor throughout every stage of the cell cycle.

Recently, Mamada *et al.* in our lab identified a new INM protein, Nemp1 (also known as TMEM194A) (see Fig. 1), which is expressed in the anterior neural plate in *Xenopus* (Mamada et al., 2009). Nemp1 has five transmembrane domains (TMs) and contains an evolutionarily conserved region A within its TMs and region B within its C-terminal region, but did not contain any known domains or motifs. They have shown that (i) Nemp1 is localized to the INM; (ii) region B faces the nucleoplasm and binds to BAF through a BAF binding site (BBS); (iii) both overexpression and knockdown of Nemp1 in *Xenopus* embryos reduce the expression of early eye-specific genes, resulting in severe eye defects; and (iv) Nemp1 activity requires region A, a Lys-Arg-rich (KR) sequence, and region B (Mamada et al., 2009). Thus, their data suggest that a proper level of Nemp1 at the INM is required for eye development. However, the molecular function of Nemp1 remains to be clarified.

In this thesis, to elucidate a new role of the NE in tissue differentiation and development, I analyzed the molecular nature of Nemp1 concerning functional roles of region A, the KR sequence, and region B using *Xenopus laevis* and mouse (*Mus musculus*) Nemp1, designated as Xl_Nemp1 and Mm_Nemp1, respectively. I found that Nemp1 colocalizes with lamins through region A, and that the KR sequence functions as NLS. Using the yeast two-hybrid

system, I identified the small GTPase Ran as a binding protein of Nemp1 and showed that Nemp1 binds to the GTP form of Ran at the INM. Co-knockdown experiments for *nemp1* and *ran* using *Xenopus* embryos showed that they are required for proper cell cycle progression and eye development. Finally, phylogenetic analysis revealed that *nemp* is conserved in eukaryotes (animals and plants) and the interaction between Nemp and Ran is also conserved. To the best of my knowledge, this study describes for the first time that Nemp1 is a new type of binding protein for Ran that is a key regulator for fundamental cellular functions.

Materials and Methods

cDNA cloning and plasmid constructs

A full-length cDNA clone (attBpBC-mKIAA0286) of *Mus musculus* (*Mm*) Nemp1 (*Mm_Nemp1*) (accession no. NM_001113211) was obtained from the Kazusa DNA Research Institute. *Mm_ran* (NM_009391) and *Xenopus laevis* (*Xl*) *ran* (NM_001086713) were isolated from the mouse 11-day embryo MatchMaker cDNA library (Clontech) and *Xenopus* total RNA at the neurula stages, respectively. *Arabidopsis thaliana* (*At*) *nemp* genes (NM_102639; NM_001037091; NM_114844) and *At_ran2* (NM_122009) were isolated from *Arabidopsis* total RNA (a gift from Dr. S. Sawa). Plasmid constructs were made with HA, Myc, and FLAG-tagged vectors, which were derived from pCSf107mT (Mii and Taira, 2009) and pCS2+. The N-terminal or C-terminal tag was indicated by the left or right position, respectively, in construct names. Two-round PCR-based mutagenesis was performed for making point-mutated, deleted, or chimeric constructs as described previously (Mamada et al., 2009). All constructs and vectors used for this study are listed in Table 1.

Yeast two-hybrid screening assay

The yeast MatchMaker Two-Hybrid System (Clontech) was used to screen the mouse 11-day embryo MatchMaker cDNA library using Mm_Bt (334 to 437a.a of Mm_Nemp1) as bait. The bait plasmid pGBKT7-Mm_Nemp1_Bt and the cDNA library were sequentially transformed into the yeast strain AH109. Transformants (9×10^6) were plated and screened on 100 mm-diameter plates with medium lacking leucine, tryptophan, and adenine. Colonies were picked and checked for ß-galactosidase production by using a filter assay with 5-bromo-4-chloro-3-indolyl-ß-D-galactopyranoside. Plasmid purification was done from the positive clones, and a second round of interaction screening was performed to confirm the interactions. The inserts from the positive clones were sequenced.

Microinjection experiments using *Xenopus* embryos

Fertilization and manipulation of *Xenopus laevis* embryos and microinjection of mRNA or morpholino oligo (MO) were carried out as described previously (Mamada et al., 2009). Embryos were staged according to the criteria of Nieuwkoop and Faber (Nieuwkoop and Faber, 1967). Antisense MOs for *Xl_nemp1* (*nemp1*MOs) (Mamada et al., 2009) or *Xl_ran* (*ran*MO) were obtained from Gene Tools LLC. *ran*MO is complementary to the sequence encompassing the translation start sites of both homoeologs of *ran (Xl_ran-a*: NM_001086713 and *Xl_ran-b*: NM_001135075) (5'-CTTGAGGTTCTCCTTGGGCTGCCAT-3'). Standard control MO (stdMO; Gene Tools LLC) was used as negative control. MOs were dissolved in water and heated at 65 °C for 10 min before use. mRNAs or MOs were injected into a dorsoanimal blastomere at the 4 cell stage, in which the injected area was fated to the anterior neural plate. Fluorescein isothiocyanate (FITC)-dextran (50 ng/embryo) and *nuclear β*-gala*ctosidase* (*nβ*-gal) mRNA (60 pg/embryo) were used as a tracer.

Whole-mount *in situ* hybridization

Whole-mount in situ hybridization (WISH) was performed according to Harland (Harland, 1991). Antisense *Xl_ran* RNA probes were transcribed with T7 RNA polymerase from SalI-linearized pGEM-T-Xl_ran.

Purification of recombinant proteins and GST pulldown assays

Glutathione S-transferase (GST) fusion constructs for Mm_Bt (GST-Mm_Bt) and Myc-tagged Mm_RanQ69L (Myc-RanQ69L) were made using pGEX6Pmcs. Purification of GST-fusion proteins and cleavage of a GST portion from GST-Ran were carried out as described previously (Shibano et al., 2007). Loading of GTP to recombinant RanQ69L was carried out in binding buffer (20 mm Tris-HCl, pH 8.0, 50 mm NaCl, 2.5 mm $MgCl_2$, 0.5%

NP-40, 1% bovine serum albumin (BSA) and 10% (v/v) glycerol) containing 2 mM GTP by incubating at room temperature for 30 min in a final volume of 50 μl, then diluting to 250 μl in binding buffer. For GST pulldown assays, GST-Mm_Bt attached to glutathione-Sepharose beads (GE Healthcare) was incubated at 4 °C for 2 h with cell lysate (see below) or with GTP-loaded RanQ69L in 300 μl of binding buffer. The beads were washed 4 times with binding buffer. Pulled down proteins were analyzed by western blotting with FluoroTrans membranes (Pall corporation) and the appropriate antibodies as described (Mamada et al., 2009).

Co-immunoprecipitation

Co-immunoprecipitation (co-IP) assays were performed essentially as described previously (Hiratani et al., 2003), with minor modifications. Injected embryos were collected at the mid blastula stage (stages 8-8.5) or the late blastula stage (stage 9), and homogenized in lysis buffer A (20 mM Tris-HCl, pH 8.0, 5 mM ethylenediamine-N,N,N',N'-tetraacetic acid (EDTA), 10% glycerol, 0.1% NP-40, 8 mM dithiothreitol (DTT), 40 μg/ml leupeptin, 20 μg/ml aprotinin, 1 mM phenylmethylsulfonyl fluoride (PMSF) for a region B containing region or lysis buffer B (50 mM Tris-HCl, pH 7.5, 5 mM EDTA, 100 mM NaCl, 0.5% NP-40, 40 μg/ml leupeptin, 20 μg/ml aprotinin, 1 mM PMSF) for full-length Nemp1. Equivalent amounts of lysates were incubated with the appropriate antibody for 1 h at 4 °C, then added with 40 μl of protein G-agarose beads (Roche), and incubated for another 1.5 h at 4 °C. The beads were washed 4 times with the same lysis buffer, added with SDS sample buffer, and boiled to elute bound proteins. Eluates were analyzed by western blotting.

Cell culture

COS-7 (derived from the kidney of African green monkey), F9 (derived from mouse testicular teratoma), and N1E115 cells (derived from mouse neuroblastoma) were cultured in

Dulbecco's modified Eagle's medium (DMEM) containing 10% fetal bovine serum (Cell Culture Bioscience) and penicillin-streptomycin (GIBCO) in 5% CO_2 incubator at 37 °C. P19 cells (derived from mouse embryonal carcinoma) were cultured in αMEM containing 10% fetal bovine serum and penicillin-streptomycin in 5% CO_2 incubator at 37 °C.

Immunofluorescence microscopy

Transfection with plasmid DNA, and confocal microscopic analysis with LSM Pascal (Zeiss) were performed as described previously (Mamada et al., 2009). Immunostaining was performed using mouse anti-Myc 9E10 (1:5000 dilution), mouse anti-HA 12CA5 (1:5000 dilution), rabbit anti-HA Y-11 (Santa Cruz; 1:200 dilution), mouse anti-pan lamin (X67, X167, X233) (Abcam; 1:25 dilution) and anti-Nup153 QE5 (Abcam; 1:250 dilution) antibodies as primary antibody and Alexa Fluor 488-, Alexa Fluor 555-, and Alexa 546-conjugated antibodies (Molecular Probes; 1:400 dilution) as secondary antibody. Nuclei were stained with SytoxGreen (Molecular Probes). For co-immunostaining with lamin, transfected cells are fixed in methanol at -20 °C.

In vitro alkaline phosphatase assays

When calf intestine alkaline phosphatase (CIAP) (New England Biolabs: NEB) was used, *Xenopus* embryos overexpressing HA-tagged Xl_Nemp1 (Xl_Nemp1-HA) were lysed in lysis buffer A. Lysates were incubated with anti-HA antibody at 4 °C for 1 h, then added with protein G-agarose beads, and incubated for another 1.5 h. The beads were washed 3 times with lysis buffer A, once with NEBuffer 3 (NEB), and incubated in NEBuffer 3 containing 0.5 u/ml of CIAP for 3 h at room temperature. When λ protein phosphatase (NEB) was used, *Xenopus* embryos overexpressing mouse Nemp1-HA (Mm_Nemp1-HA) were lysed in lysis buffer A without EDTA. Lysates were incubated with λ protein phosphatase in NEBuffer for Protein MetalloPhosphatases (NEB) for 45 min at 30 °C. Treated samples were analyzed by

western blotting with anti-HA antibody.

Measuring cell densities and ratios of mitotic cells in *Xenopus* embryos

MOs and FITC-dextran (50 ng/embryo) as a tracer were injected into the dorsoanimal region of four-cell-stage embryos. Injected embryos were collected at the late gastrula to early neurula stages (stages12.5-13), and were fixed in MEMFA (0.1 M MOPS, pH 7.4, 2 mM EGTA, 1 mM $MgSO_4$, 3.7% formaldehyde) for 2 h at room temperature, removed vitelline membranes, dehydrated in 50% and 100% methanol and stored at -20 °C. Fixed embryos were rehydrated in 75%, 50%, and 25% methanol, washed in TBT (25 mM Tris-Cl pH=7.4, 137 mM NaCl, 2.7 mM KCl, 0.1% TritonX-100, 0.2% BSA) three times and blocked with TBTS (10% lamb serum in TBT) at room temperature for 1 h. Treated embryos were incubated overnight at 4 °C with rabbit anti-phospho-Histone H3 (Ser10) antibody (Millipore; 1:500 dilution), then washed 6 times in TBT and incubated overnight at 4 °C with Alexa Fluor 555-conjugated anti-rabbit IgG antibody (Molecular Probes; 1:500 dilution) as secondary antibody. Nuclei were stained with 4',6-diamidino-2-phenylindole (DAPI). Confocal microscopic analyses were performed with LSM 710 (Zeiss). Five embryos from each experimental group were used for counting the number of nuclei and pH3-positive nuclei in more than two separate regions (a total area was more than 0.1 mm^2) of MO-injected and FITC-positive regions of each embryo. For rescue experiments, embryos were co-injected with MOs and *nemp1, ran,* or *globin* (negative control) mRNA together with *EGFP-HA* mRNA (200 pg/embryo) as a tracer, fixed at stages12.5-13, stained with DAPI and anti-HA antibody (1:10000 dilution). Nuclei were counted in EGFP-HA positive areas. The statistical significance (*P*-value) was calculated using Student's or Welch's *t*-test after comparison of the variances of a set of data by *F*-test.

Reverse transcription-polymerase chain reaction (RT-PCR) and RT-quantitative PCR (RT-qPCR)

Total RNA was isolated from F9 cells, P19 cells, N1E115 cells, or transfected COS-7 cells using Trizol (Life Technologies) and digested with RQ1 DNase (Promega). The total RNA was reverse-transcribed using SuperScriptII (invitrogen) and random primers.

RT-PCR was performed as described previously (Mamada et al., 2009) using the following primer sets:

Mm_Nemp1-F: 5′-CGGATACAAGGAGAGGTGGA-3’

and Mm_Nemp1-R: 5′-ACCAGCCTGAGGTACACACC-3’ (35 cycles);

Mm_Nemp1S-F: 5′-ATCCTGGTAGGAGGCTGGTC-3’,

and Mm_Nemp1S-R: 5′-CAGTCACCCTGCCTGCTAGT-3’ (35 cycles);

Mm_β-actin-F: 5′-TGGCACCACACCTTCTACAATGAGC-3’,

and Mm_β-actin -R: 5′-GCACAGCTTCTCCTTAATGTCACCCGC-3’ (35 cycles).

Mm_Nemp1 primers were designed for exon 8 and the 3’ UTR in exon 9 of *Mm_Nemp1*. *Mm_Nemp1S* primers were designed for exon 6 and the 3’ UTR in exon 7a of *Mm_Nemp1*.

qPCR analysis was performed using Power SYBR Green (Applied Biosystems) and a StepOnePlus real-time PCR system (Applied Biosystems) with PCR primers for *Nemp1* and *GAPDH* (glyceraldehyde 3-phosphate dehydrogenase). Nemp1-RT primers were designed for conserved sequences in *nemp1* CDSs of mouse, green monkey (*Chlorocebus sabaeus*) (XM_008003729), and human (NM_001130963). Green monkey *GAPDH* (*Cs_GAPDH*) primers were designed for conserved sequences in *gapdh* CDSs of green monkey (XM_007967342) and human (NM_001289745), and used as an internal control. Real-time PCR assays were performed in triplicate using the following primer sets:

Nemp1-RT-F: 5′-CTCCGAGAATTTTGTAACAGTCC-3′,

and Nemp1-RT-R: 5′-ATGCTCCCTAATCCATACTCCTG-3′;

Cs_GAPDH-RT-F: 5′- GAAGGTGAAGGTCGGAGTCAA-3′,

and Cs_GAPDH-RT-R: 5′- CATGTAAACCATGTAGTTGAGGTC-3′.

Results

Region A of Nemp1 plays a role in its colocalization with lamins

Region A and region B of Xl_Nemp1 and Mm_Nemp1 show 67% and 80% identities, respectively, but the KR sequence is present only in Xl_Nemp1 {Mamada, 2009 #2} (Fig. 4A). In this study, I used both Xl_Nemp1 and Mm_Nemp1, in which I utilized various deletion constructs of Xl_Nemp1 that were used for the previous study, and Mm_Nemp1 was mainly used for analyzing its interaction with Ran, respectively.

Through database searches for Mm_*Nemp1*, I found a splicing variant of *Mm_Nemp1*, which is named *Mm_Nemp1S*. Mm_Nemp1S lacks region B (Fig. 4A) and might be unique to mice. To examine the expression of *Mm_Nemp1* and *Mm_Nemp1S* in different cell types, I performed RT-PCR of cDNAs of mouse cultured cell lines, F9 (testicular teratoma), N1E115 (neuroblastoma), and P19 (embryonal carcinoma), using specific primers for each splice variants. Fig. 4B shows that *Mm_Nemp1* was strongly expressed in F9 and N1E115, whereas *Mm_Nemp1S* was strongly expressed in P19 and N1E115 (Fig. 4B), suggesting that alternative splicing of *Mm_Nemp1* is tissue type-dependent. Notably, HA-tagged Mm_Nemp1S (Mm_Nemp1S-HA) localized at the NE similar to Mm_Nemp1-HA in transfected cells (Fig. 4C), suggesting that Mm_Nemp1S could work at the NE and may compete with the full-length Nemp1. Though it should be interesting to examine Mm_Nemp1S, I focused on the full-length Nemp1.

Because region A of Xl_Nemp1 is sufficient for its nuclear envelope (NE) localization (Mamada et al., 2009), I examined the interaction of Nemp1 with lamins and the NPC component Nup153 using specific mouse monoclonal antibodies. *Nemp1* was transfected to COS-7 cells, and colocalization was analyzed by confocal analysis. Expression levels of exogenous *Mm_Nemp1-HA* were much higher than those of endogenous *nemp1* in COS-7 cells as assayed by RT-qPCR (Table 2), implying that the behavior of tagged proteins was not

affected by the endogenous protein. The data showed that the overexpression of Mm_Nemp1-HA altered the localization of endogenous lamin and that punctate staining of Mm_Nemp1 colocalized with endogenous lamins at the NE (Fig. 5B; upper panels, indicated by white arrows) but not with Nup153 at the NPC (Fig. 5B; lower panels, indicated by magenta arrows). Using deletion constructs of Xl_Nemp1, I tested which region of Nemp1 is required for its colocalization with lamins. As shown in Fig. 5C, overexpression of Xl_Nemp1-HA, Xl_ΔA-HA and Xl_ΔBt-HA altered the localization of endogenous lamin as Mm_Nemp1 and that punctated staining of Xl_Nemp1-HA and Xl_ΔBt-HA, but not Xl_ΔA-HA, colocalized with lamins. These data suggest that Nemp1 colocalizes with lamins through region A.

It was previously shown that Myc-tagged Xl_Ct and KR constructs but not Xl_Bt (see Fig. 5A) is localized to the nucleus, suggesting NLS function of the KR sequence (Mamada et al., 2009). Therefore, I systematically examined the nuclear localization activity, using GST-mRFP-HA (122 kDa as a dimer under natural conditions), which cannot be transported alone into the nucleus because NPCs block nuclear transport of diffusible proteins larger than 40-65kDa (Cautain et al., 2015). Therefore, GST-mRFP-HA was fused with short peptides related to the KR sequence, and the fusion constructs were analyzed for their ability to localize to the nucleus. As shown in Fig. 6A, GST-mRFP-HA alone was localized in the cytoplasm, whereas the SV40NLS fusion, which served as a positive control, exhibited nuclear localization. Similarly, the KR fusion proteins, KRa and KRb, which were derived from the *Xenopus* homoeologs of Nemp1, Xl_Nemp1a and Xl_Nemp1b (Mamada et al., 2009), exhibited nuclear localization, whereas the KRa(ΔR) fusion did not, indicating that both KRa and KRb sequences function as NLSs (Fig. 6A) and that the first Arg residue of the RKIKXKRAK (X is R or L) motif is required for this activity. I also analyzed a short sequence from Mm_Nemp1, whose position corresponds to that of KR in Xl_Nemp1, named KRm, though KRm does not contain a canonical NLS sequence (K-K/R-X-K/R). As expected, KRm did not elicit NLS function (Fig. 6A). However, although Mm_Bt does not have a canonical NLS sequence, HA-tagged

Mm_Bt exhibited nuclear localization (Fig. 6B; upper panels). Therefore, I analyzed NLS function of Mm_Bt using GST-mRFP-HA. This GST-mRFP-Mm_Bt-HA protein exhibited, though in a part of cells, nuclear localization (Fig. 6B), implying that Mm_Bt can exhibit NLS function under some conditions. These data suggest the possibility that the KR sequence in Xl_Nemp1 and the C-terminal region in Mm_Nemp1 as well as region A for association with lamins participate in the INM localization of Nemp1.

Nemp1 oligomerizes with itself and INM proteins thorough TMs

The INM proteins MAN1 and Emerin have been shown to be associated with each other in vitro (Mansharamani and Wilson, 2005). Therefore, I examined the interaction of Nemp1 with MAN1 and Emerin, and with itself by co-IP assays using embryos overexpressing HA-tagged Xl_Nemp1 with either Myc-tagged Xl_Nemp1, MAN1, or Emerin (Fig. 7). I found that Xl_Nemp1 forms a complex with itself and to a lesser extent with MAN1 or Emerin (Fig. 7). Deletion analysis revealed that HA-tagged WT, ΔN, ΔA, ΔBt, SP+A, and SP+TM but not ΔTM, N, or Ct were coimmunoprecipitated with Myc-tagged WT, indicating that the TMs are both required and sufficient for the oligomerization of Nemp1 (Fig. 8). The punctate staining of tagged Nemp1 at the nuclear membrane might reflect the oligomerization ability of Nemp1 (see Fig. 5B). These data suggest that Nemp1 complexes could be formed through the TMs in the NE and perhaps the ER, and might directly associate with MAN1 and Emerin or indirectly through the nuclear lamina because all three can associate with lamin.

Region B of Nemp1 directly binds to Ran

Because the previous study has shown that region B faces the nucleoplasm and is required for the eye-reducing activity of Nemp1 in *Xenopus* embryos (Mamada et al., 2009), I searched for region B-interacting proteins using the yeast two-hybrid system. I subcloned Mm_Bt as bait (Fig. 9A) for screening a mouse embryonic cDNA library. As a result, I obtained 381 positive

clones from 9×10^6 transformants and identified several candidate proteins, such as Ran and Ubc9, which interacted with Mm_Bt in yeast (Fig. 9A and Table 3). To assess the interaction of Nemp1 with Ran in the *Xenopus* embryo and also in vitro, I performed co-IP and GST pulldown assays using HA- or Myc-tagged proteins. In parallel, I also tested whether Nemp1 binds to either RanGTP or RanGDP using the GTP- and GDP-bound mutant forms Mm_RanQ69L and Mm_RanT24N, respectively. For co-IP analysis, *Xenopus* embryos were coinjected with mRNAs encoding for Mm_Bt-HA and Myc-Ran constructs. As shown in Fig. 9B, Myc-Ran (WT) and Myc-RanQ69L (GTP-bound form mutant) but not Myc-RanT24N (GDP-bound form mutant) coimmunoprecipitated with Mm_Bt-HA, suggesting that Nemp1 specifically forms a complex with RanGTP through region B in the embryo. Similarly in GST pulldown analysis, HA-Ran and HA-Myc-RanQ69L (GTP form) but not HA-RanT24N (GDP form) from embryonic lysates were pulled down by recombinant GST-Mm_Bt that was purified from bacterial lysates (Fig. 9C), indicating that Mm_Bt specifically interacts with RanGTP. To analyze direct interactions, I bacterially synthesized and purified recombinant Myc-RanQ69L by cleaving the GST moiety. Figure 9D shows that Myc-RanQ69L was pulled down by GST-Mm_Bt in comparison with GST alone, demonstrating the direct interaction between Mm_Bt and RanQ69L (GTP form).

I then examined the region of RanGTP that binds to region B. RanGTP is known to bind to both importin β and RanBP1. These interactions are disrupted in Mm_RanT42A, which has a point mutation in its effector domain (Murphy et al., 1997). In addition, the interaction between RanGTP and RanBP1 is abolished in Mm_RanΔC, which lacks the highly conserved acidic C-terminal tail of Ran (the DEDDDL sequence) (Villa Braslavsky et al., 2000). Therefore, to examine whether these regions of Ran interact with Nemp1, I performed co-IP assays using these two mutant constructs. Figure 9E shows that the ΔC mutant but not the T42A mutant co-immunoprecipitates with Mm_Bt, suggesting that region B, similarly to importin β, interacts with the effector domain of Ran. Therefore, I next tested whether region

B competes for the interaction between importin β and RanQ69L. As expected, importin β was pulled down with GST-RanQ69L, and this interaction was reduced by the addition of recombinant Mm_Bt protein at a high concentration (Fig. 9F). These data suggest that region B directly interacts with the same surface of RanGTP as importin β.

To determine a minimal Ran-binding region within the Bt region, I next performed co-IP experiments using HA-tagged deletion constructs of Mm_Bt, which were stabilized by fusing to EGFP. Interactions with Myc-Mm_Ran were detected with Bt and B but not with Ba, Bb, or Bt2 constructs (Fig. 10A). Furthermore, the deletion of the BBS (ΔBBS) in Xl_Bt abolished its interaction with Myc-Xl_Ran (Fig. 10B). These data suggest that a secondary or ternary structure of region B is required for Ran binding and that the BBS is required for Ran binding as well as BAF binding.

To examine the interaction between Nemp1 and Ran at the NE, I used full-length Nemp1 to perform co-IP and confocal microscopic analyses. As shown in Fig. 11A, HA-tagged Nemp1 was coimmunoprecipitated with Myc-tagged Ran (WT), RanQ69L, and RanΔC, but not with RanT24N and RanT42A. This data is consistent with that using the Bt region (see Fig. 9B,E). I next analyzed the localization of Nemp1 and Ran using co-immunostaining of tagged proteins in COS-7 cells by confocal microscopy. Myc-Ran alone was uniformly distributed in the nucleus (Fig. 11B; upper panels). By contrast, when coexpressed with Nemp1-HA, Myc-Ran accumulated at the nuclear periphery and colocalized with Nemp1 at the NE (Fig. 11B; lower panels). Taken together, these data suggest that Nemp1 at the INM directly interacts with RanGTP in the nucleoplasm.

Phosphorylation of Nemp1

I noticed that there were shifted bands of Mm_Nemp1 in western blotting of embryo lysates (see Fig. 12A and Supplemental Figure 1; indicated by arrowheads in the panels for Nemp1-HA). I also noticed that human Nemp1 can be phosphorylated at multiple sites

(Ser368, Ser378, Ser382, Ser424, Ser425) in the database from comprehensive analyses of phosphoproteins and phosphorylation sites (Bian et al., 2014; Daub et al., 2008; Dephoure et al., 2008; Kettenbach et al., 2011; Sharma et al., 2014). Some of these phosphorylated serines (Ser368, Ser378, Ser382) are located within region B and are evolutionarily conserved among vertebrates, and Ser-378 in the BAF binding sites is also conserved in the vertebrate paralog Nemp2 (see below). I therefore hypothesized that phosphorylation at these sites might modulate its interaction with RanGTP. I first examined whether Xl_Nemp1-HA is phosphorylated during early *Xenopus* development. Western blotting analysis of embryonic lysates containing the phosphatase inhibitor NaF revealed that shifted bands were strongly detected at the blastula stage (stage 9) when cells are actively divided, and the intensity of these bands was reduced at neurula-to-tailbud stages (stages 14, 17, and 25) when proliferation rates are declined, suggesting that the modification of Nemp1 depends on cell proliferation states (Fig. 12A). Furthermore, phosphatase treatments of immunoprecipitates or lysates abolished shifted bands of both Xl_Nemp1 (Fig. 12B) and Mm_Nemp1 (Fig. 12C), indicating that modifications of Nemp1 are phosphorylation. To seek phosphorylation sites, I mutated Ser-366, Ser376, Ser380, Ser419, and Ser420 in Mm_Nemp1, which are relevant to the phosphorylated serines in human Nemp1, to Ala or Glu to produce the non-phosphorylated construct 5SA or phosphomimetic construct 5SE, respectively. Fig. 12D and Supplemental Figure 1 show that only the upper shifted band was abolished in 5SA and 5SE mutants, suggesting that all or some of these five serine residues function as either phosphorylation sites (probable Ser366-Pro367 and Ser380-Pro381 as Cyclin/Cdk sites) or recognition sites or both, and that other phosphorylation sites exist in Nemp1. Moreover, both the 5SA and 5SE mutations abolished the interaction with Ran (Fig 12D), suggesting that all or some of these five serines of Mm_Nemp1 are involved in the interaction with Ran.

Nemp1 and Ran cooperate to function in early *Xenopus* development

Binding of Nemp1 to Ran prompted me to examine the function of their association in *Xenopus* embryos. Although the expression of *ran* is reported during the development of *Xenopus tropicalis* (Onuma et al., 2000), I re-examined this by WISH with *X. laevis* embryos using a short chromogenic reaction to reduce staining intensity. Relatively strong *ran* expression was detected within the animal pole region at the four-cell stage, then in the anterior neural plate at the neurula stage, and within the head region including the otic vesicles, branchial arches, and the tail region at the tailbud stage (Fig. 13A). These expression patterns were similar to those of *nemp1* in *Xenopus* embryos (Mamada et al., 2009), consistent with the interaction of Nemp1 with Ran.

To elucidate the cooperative role of Nemp1 and Ran in *Xenopus* eye development, I knocked down both Nemp1 and Ran activities by injecting antisense morpholino oligos (MOs), *nemp1*MOs (Mamada et al., 2009) and *ran*MO. I designed *ran*MO to be complementary to the sequence encompassing the translation start sites of both *X. laevis* homoeologs of *ran*. I confirmed that *ran*MO specifically inhibited protein synthesis from *Xl_Ran-Myc* mRNA containing the MO target sequence but not from *Myc-Xl_Ran* mRNA without the target (Fig. 13B). Injection of *nemp1*MOs or *ran*MO alone exhibited weak activity for inhibiting eye development, whereas the co-knockdown with *nemp1* and *ran* elicited more severe eye defects than either individual knockdown alone (Fig. 13C). This data suggests the functional interaction between Nemp1 and Ran.

Because *nemp1* and *ran* are expressed in the anterior neural plate and eye vesicles, in which cells highly proliferate, I next performed loss-of- and gain-of-function experiments for *nemp1* and *ran* to examine their effects on cell densities and ratios of mitotic cells at the late gastrula to early neurula stages (stages12.5-13) (Fig. 14 and 15). Injection of *nemp1*MOs (10 or 20 ng/embryo) but not stdMO or *ran*MO significantly reduced cell densities (Fig. 14A,B) and was likely to increase nuclear size (compare panels a' and d' in Fig. 14A). Co-injection of *ran*MO

with *nemp1*MOs further reduced cell densities compared to single knockdowns (Fig. 14B). The reduction by *nemp1*MOs was significantly rescued by low doses of *nemp1* mRNA (Fig. 14C) and the reduction by both MOs tended to be rescued by *nemp1*and *ran* mRNAs (Fig. 14D). These data suggest again the functional synergism between Nemp1 and Ran. High doses of *nemp1* mRNA as well as nemp1 MO reduced cell densities (Fig. 14E), suggesting that a proper level of Nemp1 is required for normal functions similar to eye phenotypes (Mamada et al., 2009). Supporting the reduction in cell density, single knockdown of *nemp1* or co-knockdown of *nemp1* and *ran* as well as overexpression of *nemp1* by mRNA injection tended to decrease mitotic rates, which were determined using anti-phosphohistone-H3 antibody (Fig. 15A,B). Thus, it is likely that the reduction in cell density at the neurula stage is caused by the reduction in cell cycle progression by knockdown or overexpression of Nemp1 and Ran. Taken together, the data suggest that *nemp1* and *ran* function cooperatively in proper cell cycle progression and eye development in *Xenopus*.

Interaction between Nemp and Ran is evolutionally conserved in *Arabidopsis*

Although the data in this study suggest the role of Nemp1 in eye development, *nemp1* is also expressed in other tissues (see Fig. 13A) and exists in other organisms, such as *Drosophila* and *Caenorhabditis elegans* (Mamada et al., 2009), implying a role of Nemp1 in tissues other than the eyes. To gain insight into a role of the interaction between Nemp and Ran in other organisms, I examined the evolutionary conservation of Nemp proteins among various organisms including plants as well as that of the interaction between Nemp1 and Ran. The sequences containing regions A and B are annotated in the Pfam database as an evolutionary conserved domain of unknown function (DUF) named DUF2215 (the protein family name is PF10225) (http://pfam.sanger.ac.uk/) (Fig. 16). Using the DUF2215 motif as well as the entire amino acid sequence of Xl_Nemp1 as queries, I performed BLAST searches and identified orthologs from metazoans to plants. Phylogenetic and syntenic analyses revealed that (i)

Nemp2 (TMEM194B) proteins are vertebrate paralogs (Fig. 17A), whereas the *Xenopus* species appear to lack it (Fig. 17B); (ii) *Arabidopsis thaliana* has three paralogs, At_Nemp-A, -B, and –C (Fig. 17A); (iii) At_Nemp-A is relative strongly expressed in shoot apex and At_Nemp-B and-C are expressed in guard cells (https://www.arabidopsis.org/) and (iv) In plants, region A is more conserved to that of metazoan Nemp than region B is (Table. 4).

To examine conservation of the interaction between Nemp and Ran, I performed co-ip assays for the three *Arabidopsis* Nemp proteins, At_Nemp-A, At_Nemp-B, and At_Nemp-C (Fig. 18), as well as for At_Ran2. At_Ran2 is one of the four Ran proteins in *Arabidopsis* and is the most related to vertebrate orthologs. Because region B of At_Nemp proteins are not well defined by comparison to vertebrate Nemp1 due to low sequence conservation, the entire C-terminal regions downstream of the last TM (named Ct) were used for co-ip experiments. As shown in Fig. 18A and B, At_Ran2 coimmunoprecipitated significantly with At_Nemp-A, weakly with At_Nemp-B, and barely with At_Nemp-C. Intriguingly, Fig. 18C shows that Mm_Bt did not interact with At_Ran2, and conversely, At_Nemps did not interact with Mm_Ran, suggesting that Nemp and Ran coevolved to interact with each other. These data suggest that, despite the fact that sequence conservation in region B is relatively low between vertebrates and plants, the interaction between Nemp and Ran itself is evolutionally conserved. Thus, the role of Nemp as a RanGTP-interacting protein might be related to basic cellular functions in eukaryotes, such as the nuclear transport system and NE assembly.

Discussion

Localization of Nemp1 at the INM

A previous study has shown that the signal peptide and TMs are necessary and sufficient for Nemp1 to localize at the NE (Mamada et al., 2009). The localization of nuclear membrane proteins to the INM is postulated to be facilitated by the following two mechanisms: diffusion-retention and importin α/β-mediated transport. For example, in the former case, MAN1 moves diffusely to the INM from the ER and is retained by the binding of its N-terminal domain to lamins (Mansharamani and Wilson, 2005; Wu et al., 2002). In the latter case, Heh2, a yeast homolog of vertebrate LEM2, contains a canonical NLS-like sequence within its N-terminal nucleoplasmic domain and is transported to the INM by importin α/β complexes (King et al., 2006). I have shown that Nemp1 colocalizes with lamina through region A (Fig. 5), and that the C-terminal region of Nemp1 exhibits nuclear localization activity (Fig. 6). My data suggest that Nemp1 localizes at the INM via both diffusion-retention and NLS-dependent transport mechanisms.

Binding of region B to RanGTP

I have found that Nemp1 specifically interacts with RanGTP via region B (Figs. 9, 10) and that this interaction is conserved in *C. elegans* (Li et al., 2004) and plants (Fig. 18). RanGTP is known to interact with various factors that are associated with nuclear transport and spindle formation, including importins, exportins, RanBP1, and RanBP2. The following two types of RanGTP-binding motifs have been reported: importin β and RanBP1/2 motifs (Chook and Blobel, 1999; Vetter et al., 1999). As the conserved motif of region B is different from these two types, Nemp1 might represent a new type of RanGTP-binding motif. Furthermore, Nemp1 is the first identified nuclear membrane protein reported to bind to RanGTP.

What is the function of Nemp1? I have shown that the coexpression of Mm_Nemp1 promotes the accumulation of Ran at the nuclear envelope (NE) in COS-7 cells (Fig. 11B). Based on this observation, it is possible to speculate that the role of Nemp1 is to promote the accumulation of RanGTP at the nuclear periphery. This idea is supported by observations in *C. elegans* and *Arabidopsis* that endogenous Ran localizes at the NE during interphase (Bamba et al., 2002; Ma et al., 2007). The peripherally biased distribution of RanGTP in the nucleus might be important for efficient dissociation of cargo-importin complexes, which are imported through the NPC and could immediately encounter enriched levels of RanGTP.

A previous study revealed that Nemp1 interacts with BAF through the BBS and that the BBS is required for the eye-reducing activity of overexpressed Nemp1 (Mamada et al., 2009). Recently, it was reported that in the absence of DNA, there is no interaction of BAF with BBS-containing proteins, such as CRX and MAN1 (Huang et al., 2011). Nemp1 might also indirectly bind to BAF via DNA. In this study, I have shown that the deletion of BBS abolishes the interaction of the Bt region with Ran (Fig. 10B). Furthermore, both BAF (Mamada et al., 2009) and Ran accumulate at the nuclear periphery via Nemp1 (Fig. 11B). These data suggest that the eye-reducing activity of overexpressed Nemp1 is mediated through its interactions with BAF and Ran. Although Nemp1 is likely to play a role in promoting the accumulation of Ran at the nuclear periphery, the excessive accumulation of Ran as well as of BAF at the nuclear periphery by overexpression of Nemp1 likely perturbs their normal functions. Conversely, the co-knockdown of *nemp1* and *ran* elicits reduction of cell density and eye defects more significantly than the individual knockdown for *nemp1*, supporting their functional interaction.

Phosphorylation of Nemp1

Some nuclear lamina proteins (lamins and INM proteins) are reported to be phosphorylated in the prophase of mitosis, resulting in their dysfunction during the NE breakdown. For example,

lamin filaments are depolymerized upon phosphorylation of lamin B proteins (Hocevar et al., 1993; Peter et al., 1990), and the LBR (lamin B receptor) is dissociated from chromatin upon phosphorylation of LBR (Tseng and Chen, 2011). Similar to these NE proteins, the data suggest the possibility that phosphorylation of Nemp1 occurs in mitosis (Fig. 12A,B,C). In addition, serine residues at possible phosphorylation sites are involved in the interaction with Ran (Fig. 12D). Taken together, the data in this study (Fig. 12) and previous reports (Bian et al., 2014; Daub et al., 2008; Dephoure et al., 2008; Kettenbach et al., 2011; Sharma et al., 2014) suggest the possibility that phosphorylation of Nemp1 occurs during M phase, which reduces its interaction with RanGTP. During mitosis, RanGTP is concentrated near the chromosomes to recruit spindle assembly factors (SAFs) for spindle formation and NPCs for NE reassembly, events that are important for proper mitotic progression. Therefore, it is likely that the phosphorylation of Nemp1 prevents the interruption of the accumulation of RanGTP to the chromosome during the M phase. In addition, two phosphorylated serines, Ser378 and Ser382, are located in the BBS of region B (see Fig. 16). This suggests the possibility that the phosphorylation of Nemp1 also affects the binding of BAF during the M phase. It is important to examine relationships between phosphorylation of Nemp1 and its interactions with Ran and BAF.

Role of Nemp1 in *Xenopus* eye development

How is Nemp1 involved in eye development? While there seems to be no direct relationship between the function of Nemp1/Ran and eye development, I propose two possibilities. First, Nemp1 might regulate the nuclear transport of eye-specific transcription factors. In humans, the importin β family consists of 20 members (Hahn and Schlenstedt, 2011), of which importin 13 is known to function in the import of several transcriptional factors, such as Pax6 and Crx, which are important for eye development (Ploski et al., 2004). Knockdown of *nemp1* reduced the expression of early eye marker genes, *rax* and *pax6*

(Mamada et al., 2009). Therefore, it is conceivable that Nemp1 controls importin13-mediated transport. The second possibility is that Nemp1 is associated with cell proliferation, which is important for eye development. This possibility is based on the fact that knockdown of *nemp1* caused the reduction of cell densities (Fig. 14A,B), and that expression patterns of *nemp1* and *ran* (Fig. 13A) are similar to those of cell cycle regulators, *cyclin D1*, *cyclin E*, and *cdk4* (Vernon and Philpott, 2003). These data suggest that increased levels of Nemp1 and Ran are necessary for maintaining an actively proliferative state (Fig. 19), in which nuclear uptake is more likely to be active than in non-proliferating cells (Feldherr and Akin, 1994).

The ancient origin of Nemp1

The phylogenetic analysis revealed that Nemp is conserved in animals, choanoflagellates, and plants (Fig. 17), suggesting that Nemp is conserved in eukaryotes. SUN domain proteins are also conserved in choanoflagellates (Wilson and Dawson, 2011) and plants (Graumann and Evans, 2010). However, although the NE is a fundamental feature in eukaryotes, nuclear lamina proteins are not necessarily conserved in eukaryotes. For example, lamin is a major component of the nuclear lamina and plays various roles in the structure and function of the NE, but is only conserved in metazoans (Peter and Reimer, 2012). Instead, plants have lamin-like analogues, called *crowded nuclei* (CRWN) 1 and 4 [originally named *little nuclei* (*linc*)], which play predominant roles in nuclear morphology (Ciska et al., 2013; Dittmer et al., 2007; Sakamoto and Takagi, 2013). Similarly, nuclear membrane proteins, such as LBR, KASH domain proteins and LEM domain proteins, are not present in plants. Compared to INM and ONM proteins and nuclear lamina components, nuclear transport proteins are well conserved in eukaryotes. For example, Ran and its associated proteins, RanGAP1, NTF2, RanBP1, and RCC1, as well as importin β and exportin 1 are all conserved in eukaryotes (Mans et al., 2004). Thus, Nemp might be one of ancient and fundamental INM proteins involved in cellular processes including nuclear transport.

Conclusion

In this study, I have shown three main points for the molecular nature of the inner nuclear membrane (INM) protein Nemp1. Firstly, I have demonstrated that Nemp1 interacts with RanGTP through region B in the nucleoplasm on the INM. This interaction is unique because the conserved motif of region B is distinct from the two well-known RanGTP binding motifs from importin β and RanBP1. Secondly, I have shown that physical interactions between Nemp1 and Ran are evolutionarily conserved from eumetazoans to plants. Thirdly, the interaction between Nemp1 and Ran is required for proper cell proliferation and eye development in *Xenopus*. Because *nemp1* and *ran* are co-expressed in various tissues including the eyes, Nemp1 is likely to play general roles in regulating the nuclear transport of proteins by interacting with RanGTP during cellular proliferation and differentiation. Taken together, I conclude that the inner nuclear membrane protein Nemp1 represents a new type of RanGTP-binding protein in eukaryotes.

Acknowledgements

I would like to express my immeasurable gratitude to Dr. Masanori Taira (Department of Biological Sciences, Graduate school of Science, The University of Tokyo) for his valuable advises, sensible suggestions, and great encouragements in my doctoral course and after withdrawal from the doctoral program with the completion of course requirement. I would also like to my deep gratitude to Dr. Shin-Ichiro Takahashi (Department of Animal Sciences and Agricultural Biological Chemistry, Graduate School of Agriculture and Life Sciences, The University of Tokyo) for his strong encouragement in various aspects of my research life and long support for writing the thesis. I thank Dr. Hisashi Koga for Mm_TMEM194A plasmid; Dr. Hiroshi Sasaki for a mouse embryonic cDNA library; Dr. Fumihiko Hakuno for yeast two hybrid screening; Dr. Shin-ichiro Sawa for *Arabidopsis* total RNA; Dr. Satomi Tanaka for importin 13 plasmid; Dr. Shoji Tajima for F9, P19, and N1E115 cells and helpful suggestions about purifying recombinant proteins; Dr. Yumi Izutsu for frozen sectioning of *Xenopus* embryos; and Dr. Mariko Kondo for critical reading of the manuscript published in PLOS One. I also thank Dr. Hiroshi Mamada for Nemp1 constructs; Ms. Yumeko Satou and Dr. Takayoshi Yamamoto for supporting my experiments; Ms. Yuuki Goya and Dr. Norihiro Sudou for strong encouragements; and other members of Taira Laboratory for helpful comments and discussions.

Tables

Table 1 List of plasmid constructs used in this paper

Plasmid names	Purposes*	Reference and Commnets
pCSf107_4HAmT	Vector	N-terminal 4 HA tags
pCSf107_MTmT	Vector	N-terminal 6 Myc tags
pCSf107_2FTmT	Vector	N-terminal 2 FLAG tags
pCS2mcs4HAmcsT	Vector	C-terminal 4 HA tags
pCS2mcsMTmcsT	Vector	C-terminal 6 Myc tags
pCS2mcs2FTmcsT	Vector	C-terminal 2 FLAG tags
pCSf107GFPgmT	Vector	Gly(14) linker after EGFP
pCSf107GSTmRFP-HA	Vector	
pCSf107GSTmRFP-SV40NLS-HA	IF	
pCSf107GSTmRFP-KRa-HA	IF	
pCSf107GSTmRFP-KRb-HA	IF	
pCSf107GSTmRFP-KRa(dR)-HA	IF	
pCSf107GSTmRFP-KRm-HA	IF	
pCSf107GSTmRFP-Mm_Bt-HA	IF	
pGBKT7-Mm_Bt	Yeast 2 hybrid	aa 334-437
pGAD10-Mm_Ran	Yeast 2 hybrid	3B1-2 (clone)
pGEX6Pmcs-Mm_Bt	GST-pull down	
pCSf107_4HAmT-Mm_Ran	GST-pull down	
pCSf107_4HAmT-Mm_Ran_T24N	GST-pull down	
pCSf107_4HAMTmT-Mm_Ran_Q69L	GST-pull down	
pCS2mcs4HAmcsT-Mm_Bt	co-IP, IF	
pCSf107_MTmT-Mm_Ran	co-IP	
pCSf107_MTmT-Mm_Ran_T24N	co-IP	
pCSf107_MTmT-Mm_Ran_Q69L	co-IP	
pGEX6Pmcs-Myc-Mm_Ran_Q69L	GST-pull down	
pCSf107GFPgmT-Mm_Bt-HA	co-IP	aa 334-437
pCSf107GFPgmT-Mm_B-HA	co-IP	aa 334-403
pCSf107GFPgmT-Mm_BaHA	co-IP	aa 334-371
pCSf107GFPgmT-Mm_Bb-HA	co-IP	aa 362-403
pCSf107GFPgmT-Mm_Bt2-HA	co-IP	aa 404-437
pCSf107_MTmT-Xl_Ran	co-IP	
pCSf107GFPgmT-Xl_Bt-HA	co-IP	
pCSf107GFPgmT-Xl_Bt_ΔBBS-HA	co-IP	
pCSf107GFPgmT-At_Nemp1-A_Ct-HA	co-IP	aa 319-476
pCSf107GFPgmT-At_Nemp1-B_Ct-HA	co-IP	aa 344-498
pCSf107GFPgmT-At_Nemp1-C_Ct-HA	co-IP	aa 344-457
pCSf107_MTmT-At_Ran2	co-IP	
pCS2mcs4HAmcsT-Xl_Nemp1b	co-IP, injection	
pCS2mcs4HAmcsT-Mm_Nemp1	IF, co-IP	
pCS2mcs4HAmcsT-Mm_Nemp1	IF, co-IP	
pCS2mcs4HAmcsT-Mm_Nemp1_5SA	co-IP	
pCS2mcs4HAmcsT-Mm_Nemp1_5SE	co-IP	
pCS2mcs4HAmcsT-Xl_Nemp1a	IF. co-IP	
pCS2mcs4HAmcsT-Xl_Nemp1a_ΔA	IF. co-IP	
pCS2mcs4HAmcsT-Xl_Nemp1a_ΔBt	IF. co-IP	
pCS2+MAN1-myc	co-IP	mRNA preparation by Mamada
pCS2+emerin-myc	co-IP	mRNA preparation by Mamada
pCS2mcsMTmcsT-Xl_Nemp1a	co-IP	Mamada et al., 2009
pCS2mcsMTmcsT-Xl_Nemp1a_ΔN	co-IP	Mamada et al., 2009
pCS2mcsMTmcsT-Xl_Nemp1a_ΔA	co-IP	Mamada et al., 2009
pCS2mcsMTmcsT-Xl_Nemp1b_ΔTM	co-IP	aa 1-147 + aa 317-434
pCS2mcsMTmcsT-Xl_Nemp1a_ΔBt	co-IP	Mamada et al., 2009
pCS2mcsMTmcsT-Xl_Nemp1b_N	co-IP	aa 1-147
pCS2mcsMTmcsT-Xl_Nemp1a_SP+A	co-IP	Mamada et al., 2009

pCS2mcsMTmcsT-Xl_Nemp1a_SP+TM	co-IP	Mamada et al., 2009
pCS2mcsMTmcsT-Xl_Nemp1a_Ct	co-IP	Mamada et al., 2009
pCSf107_MTmT-Mm_Ran_T42A	co-IP	
pCSf107_MTmT-Mm_Ran_ΔC	co-IP	
pCSf107_2FTmT-importin β1	GST-pull down	
pCS2mcsMTmcsT-Xl_Ran	Injection	
pGEM-T-Xl_ran	WISH	

*Abbreviations: co-IP, co-immunoprecipitation; IF, Immunofluorescence; injection, mRNA injection for functional analysis; WISH, whole mount *in situ* hybridization.

Table 2 Comparison of expression levels between endogenous and exogenous Nemp1 mRNAs in DNA-transfected COS-7 cells

DNA constructs	relative expression levels[a]
Mock[b]	1.00±0.05
Mm_Nemp1-HA[c]	686±10

a, Values were obtained from 3 independent dishes.
b, Expression levels of endogenous *Nemp1*
c, The value was divided by the transfection efficiency (30.9%; the total number of cells counted from four different areas was 6,199).

Table 3 Results of yeast two hybrid screening

Gene names	Functions	The number of positive clones	Rechecked in yeasts	
			Prey only[a]	Bait-prey interactions[b]
Ubc9	SUMO E2 enzyme	19	–	+
Ran	small GTPase	10	–[c]	++[c]
Wnk1	serine/threonine kinase	3	++	++
Paics	nucleotide metabolism enzyme	2	N. D.	N. D.
Coronin1B	actin binding protein	1	–	+
MRG15	chromatin protein	1	–	–

a, colony formation (in duplicate) of yeast AH109 cells transformed with only a prey plasmid on plates lacking tryptophan, leucine, and adenine.

b, colony formation (in duplicate) of yeast AH109 cells transformed with both bait and prey plasmids on plates lacking tryptophan, leucine, and adenine.

++, two colonies were formed; +, one colony was formed; -, no colony was formed; N.D., not determined.

c, this data was also presented in Fig. 9A.

Table 4 Pair-wised comparisons of region A and B of Nemp proteins in organisms from vertebrates, invertebrates to plant

region B				region A																					
				vertebrates											invertebrates								plant		
				Nemp1							Nemp2				Nemp								A	B	C
				Hs	Mm	Gg	Xl-a	Xl-b	Xt	Dr	Hs	Mm	Gg	Dr	Ce	Dm	Nv	Sk	Sp	Ci	Bf	Mb	At	At	At
vertebrates	Nemp1		Hs		89	71	68	66	70	63	40	38	42	38	45	37	39	35	40	35	53	20	18	19	19
			Mm	93		71	67	65	69	62	41	39	41	37	46	39	38	37	39	35	49	19	18	22	22
			Gg	81	74		68	65	67	63	39	38	38	34	42	40	40	38	46	35	52	16	15	16	21
			Xl-a	84	80	79		91	95	58	41	38	42	37	46	40	39	32	43	37	53	16	14	16	18
			Xl-b	87	83	76	89		93	59	37	38	40	35	45	38	41	30	41	33	52	16	15	17	16
			Xt	89	81	81	93	93		59	40	41	40	36	47	41	41	32	42	36	55	17	15	18	17
			Dr	71	69	64	71	70	73		41	37	37	35	44	35	38	34	42	42	46	21	18	19	20
	Nemp2		Hs	53	47	53	53	56	56	47		77	54	32	37	32	33	27	32	34	35	25	14	17	14
			Mm	57	51	61	57	57	57	51	71		50	27	37	34	32	28	29	31	40	22	12	19	16
			Gg	60	56	57	56	53	56	53	57	60		32	38	34	35	24	32	28	40	20	11	16	10
			Dr	56	51	56	53	51	54	46	47	49	47		27	27	30	27	27	31	30	16	13	13	12
invertebrates	Nemp		Ce	31	31	30	31	31	30	30	22	24	27	30		38	39	32	39	37	44	18	18	16	13
			Dm	40	42	40	38	38	39	42	33	33	35	36	30		35	27	35	28	39	19	15	17	16
			Nv	50	49	46	46	44	46	43	37	36	39	43	31	36		34	36	37	47	22	18	18	18
			Sk	58	59	56	56	58	56	54	46	42	46	46	41	42	54		39	37	44	19	14	17	16
			Sp	51	50	54	50	49	53	50	40	46	46	49	34	37	50	52		35	54	15	19	15	13
			Ci	59	57	57	56	53	56	50	41	40	39	43	39	33	49	54	49		37	19	16	17	16
			Bf	44	39	38	40	41	41	41	33	37	37	30	29	33	37	37	40	36		17	16	17	12
			Mb	16	17	13	14	16	14	14	15	14	13	12	11	12	12	17	16	16	12		15	16	11
plant		A	At	13	14	8	15	13	15	8	7	8	7	8	6	10	5	8	9	8	5	11		44	44
		B	At	14	16	12	13	14	13	9	9	11	9	9	5	10	5	11	7	11	10	7	14		52
		C	At	11	13	7	11	11	11	7	8	11	8	10	3	7	2	14	11	11	8	3	16	38	

Percent identities of amino acid sequences of region A (the upper-right half) and B (the lower-left half) between each pair of organisms are shown.

Abbreviations of species (common name): At, *Arabidopsis thaliana*; Bf, *Branchiostoma floridae* (Florida lancelet); Ce, *Caenorhabditis elegans* (nematode); Ci, *Ciona intestinalis* (ascidian); Dm, *Drosophila melanogaster*; Dr, *Danio rerio* (zebrafish); Gg, *Gallus gallus* (chick); Hs, *Homo sapiens* (human); Mb, *Monosiga brevicollis* (choanoflagellate); Mm, *Mus musculus* (mouse);Nv, *Nematostella vectensis* (sea anemone); Sk, *Saccoglossus kowalevskii*; Sp, *Strongylocentrotus purpuratus*; Xl, *Xenopus laevis* (African clawed frog); Xt, *Xenopus tropicalis* (western clawed frog).

Figures

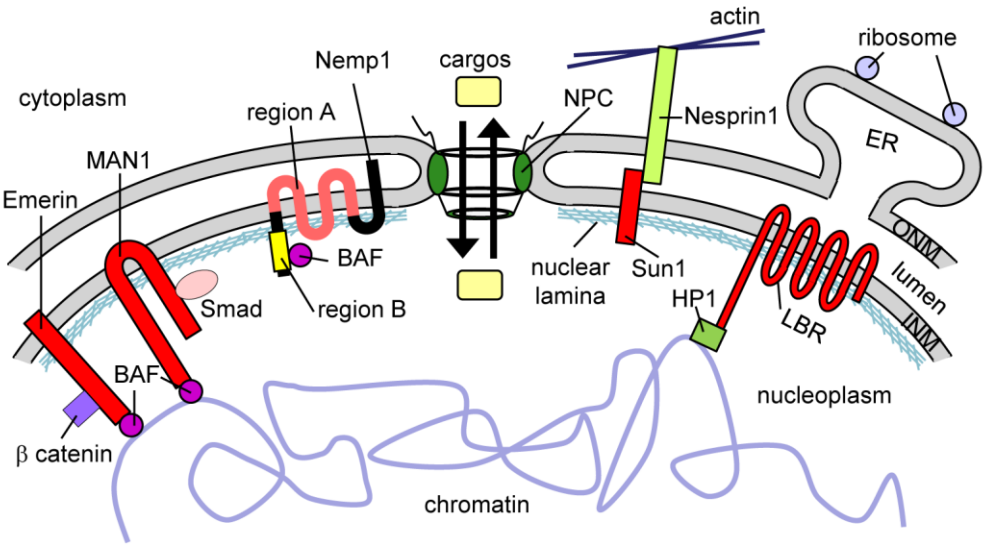

Figure 1 Structure of the nuclear envelope

The nuclear envelope is composed of two layers of membranes, the outer nuclear membrane (ONM), and the inner nuclear membrane (INM). The ONM is continuous with the endoplasmic reticulum (ER). The INM is tightly associated with a fibrous protein meshwork called the nuclear lamina that contains intermediate filaments, lamins and membrane proteins. Nuclear pore complexes (NPCs) mediate nuclear import and export of cargos (proteins and RNAs) as indicated by black arrows. Heterochromatin is mainly localized at the nuclear periphery. Emerin and MAN1 bind to chromatin through BAF (barrier to autointegration factor). LBR interacts with chromatin through HP1. Sun1 binds to Nesprin1 to link the nucleoskeleton to the cytoskeleton. The N-terminus and the C-terminus of Nemp1 is oriented to the lumen and the nucleoplasm, respectively, and Nemp1 interacts with BAF (Mamada et al., 2009).

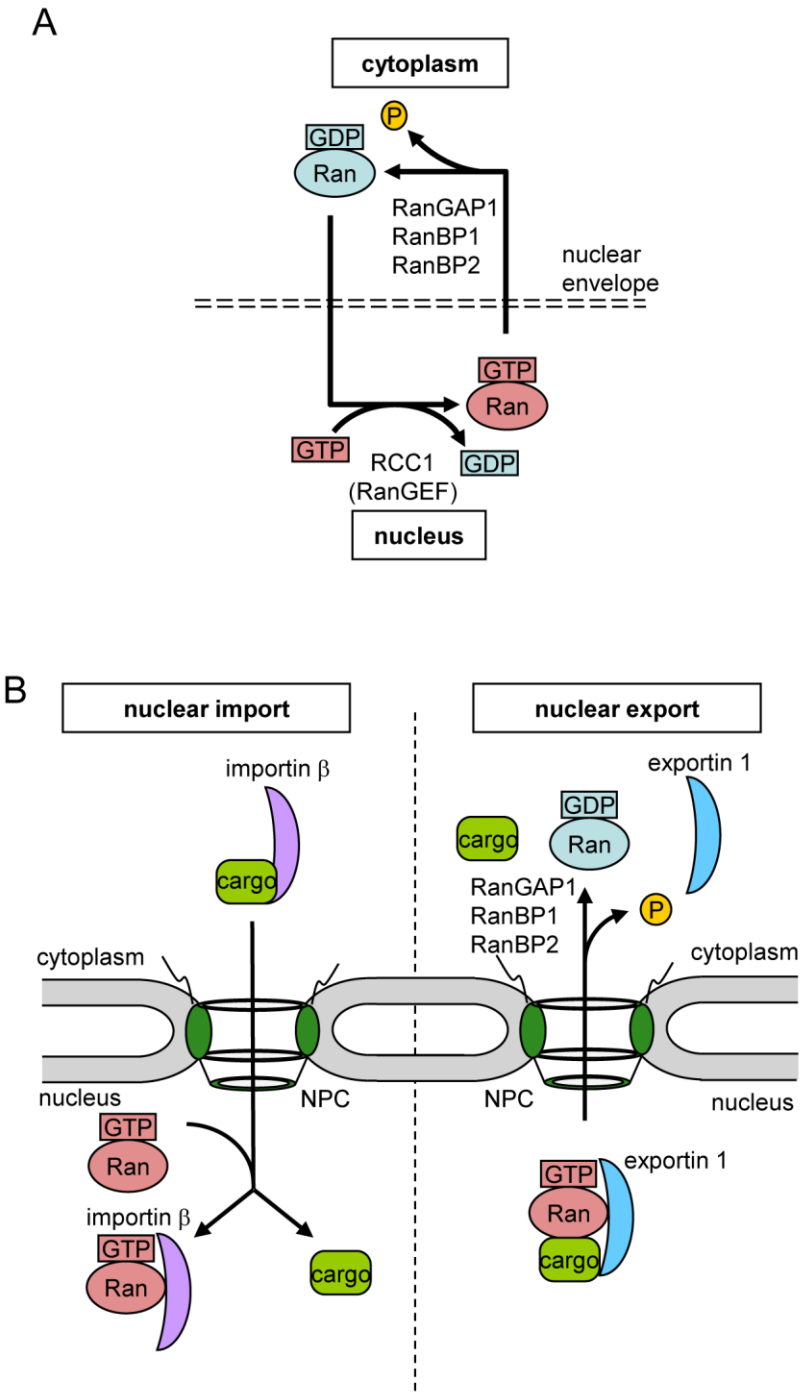
A
cytoplasm
P
GDP
Ran
RanGAP1
RanBP1
RanBP2
nuclear
envelope
GTP
Ran
GTP
RCC1
(RanGEF)
GDP
nucleus
B
nuclear import
nuclear export
importin β
exportin 1
cargo
GDP
Ran
RanGAP1
RanBP1
RanBP2
P
cytoplasm
cytoplasm
nucleus
NPC
NPC
nucleus
GTP
Ran
exportin 1
importin β
GTP
Ran
cargo
GTP
Ran
cargo

Figure 2

Figure 2 Regulation of nuclear transport by the small GTPase Ran

(A) Compartmentalization of RanGDP and RanGTP. Small GTPase Ran exists in two forms, the GDP-bounded from (RanGDP) and the GTP-bounded form (RanGTP). RanGDP and RanGTP are enriched in the cytoplasm and the nucleus, respectively. This compartmentalization is maintained by RCC1 (RanGEF) in the nucleus and RanGAP1 and its cofactors (RanBP1, and RanBP2) in the cytoplasm.

(B) Diagram of nuclear transport. Left panel, nuclear import. In the cytoplasm, a cargo is interacted with importin β and transported into the nucleus. In the nucleus, RanGTP binds to importins to dissociate the cargo from importin β. Right panel, nuclear export. In the nucleus, exportin 1 forms a complex with a cargo and RanGTP, and transports the cargo to the cytoplasm. In the cytoplasm, RanGAP1 and its cofactors, RanBP1 and RanBP2, activate Ran GTPase activity to convert RanGTP to RanGDP, resulting in the dissociation of the ternary complex.

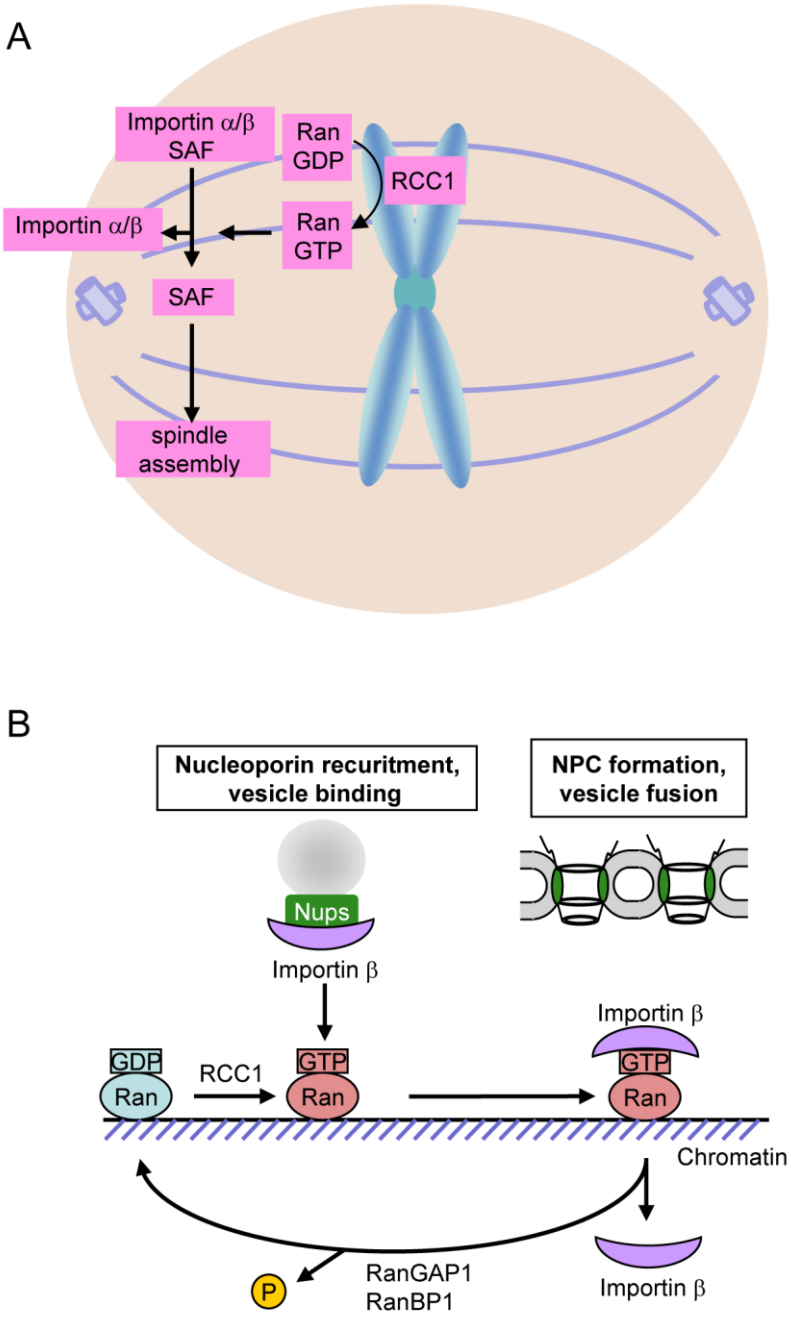
A
Importin α/β
SAF
Ran
GDP
RCC1
Importin α/β
Ran
GTP
SAF
spindle
assembly
B
Nucleoporin recuritment,
vesicle binding
NPC formation,
vesicle fusion
Nups
Importin β
Importin β
GDP
Ran
RCC1
GTP
Ran
GTP
Ran
Chromatin
P
RanGAP1
RanBP1
Importin β

Figure 3

Figure 3 Roles of the small GTPase Ran in mitosis

(A) Regulation of spindle assembly by Ran. Importin α/β bind to SAFs (spindle assembly factors) to suppress the activity of SAFs. Around the chromosome, RanGTP is concentrated due to chromatin-bounded RCC1, which converts RanGDP to RanGTP. RanGTP releases SAFs from importin α/β to activate SAFs, resulting in spindle assembly around chromosome.

(B) Control of nuclear re-assembly in mitosis by Ran. Importin β binds to nucleoporins, such as Nup107, Nup153, and Nup358, to form inhibitory complexes for inhibiting assembly of NPCs (nuclear pore complexes). Locally concentrated RanGTP generated by chromatin-bound RCC1 binds to importin β to release the nucleoporins from the inhibitory complexes, allowing assembly of NPCs and vesicle fusion. Nups. nucleoporins. (modified from Clarke and Zhang, 2008)

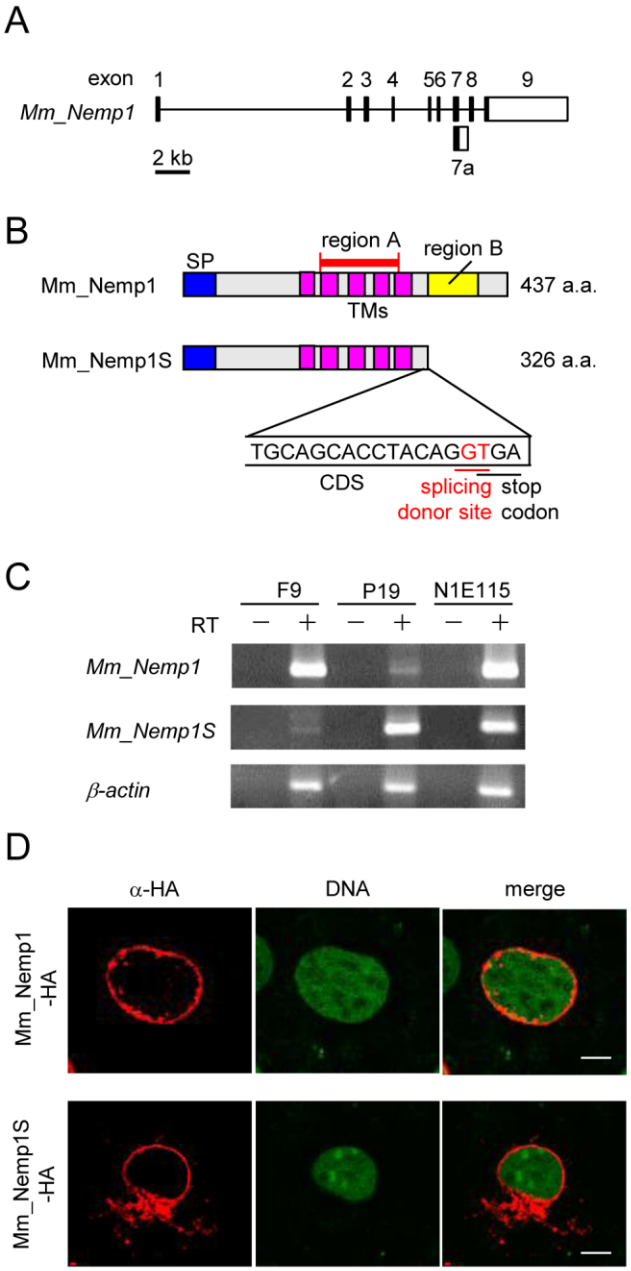
A
exon 1 2 3 4 5 6 7 8 9
Mm_Nemp1
2 kb
7a
B
region A
region B
SP
Mm_Nemp1
437 a.a.
TMs
Mm_Nemp1S
326 a.a.
TGCAGCACCTACAGGTGA
CDS
splicing donor site
stop codon
C
F9
P19
N1E115
RT
− + − + − +
Mm_Nemp1
Mm_Nemp1S
β-actin
D
α-HA
DNA
merge
Mm_Nemp1 -HA
Mm_Nemp1S -HA

Figure 4

Figure 4 Expression and subcellular localization of Mm_Nemp1 and its splicing variant, Mm_Nemp1S

(A) Gene structure of *Mm_Nemp1*. The exon-intron structure is schematically represented. Exon 7a is used as the last exon for *Mm_Nemp1S* mRNA. Black boxes, exons; white boxes, untranslated region (UTR); lines, introns.

(B) Diagram of primary structures of Mm_Nemp1 and Mm_Nemp1S. Blue, signal peptides (SP); magenta transmembrane domains (TMs); yellow boxes, region B. In exon 7a, the 5' portion of the seventh intron is retained, generating an in-frame stop codon (TGA) just after the intron donor site. As a result, Mm_Nemp1S lacks region B. a.a., amino acid residues.

(C) RT-PCR analysis of *Mm_Nemp1* and *Mm_Nemp1S* expression in F9, P19, and N1E115 cells. F9, mouse testicular teratoma cells; P19, mouse embryonal carcinoma cells; N1E115, mouse neuroblastoma cells; RT, RT-PCR with (+) or without (-) reverse transcription; β-actin, internal control.

(D) Nuclear envelope localization of MmNemp1 and Mm_Nemp1S proteins. COS-7 cells were transfected with *Mm_Nemp1-HA* or *Mm_Nemp1S-HA* expression construct as indicated, fixed, and stained with anti-HA antibody (red) and SYTOX Green for DNA. Scale bars, 5 μm.

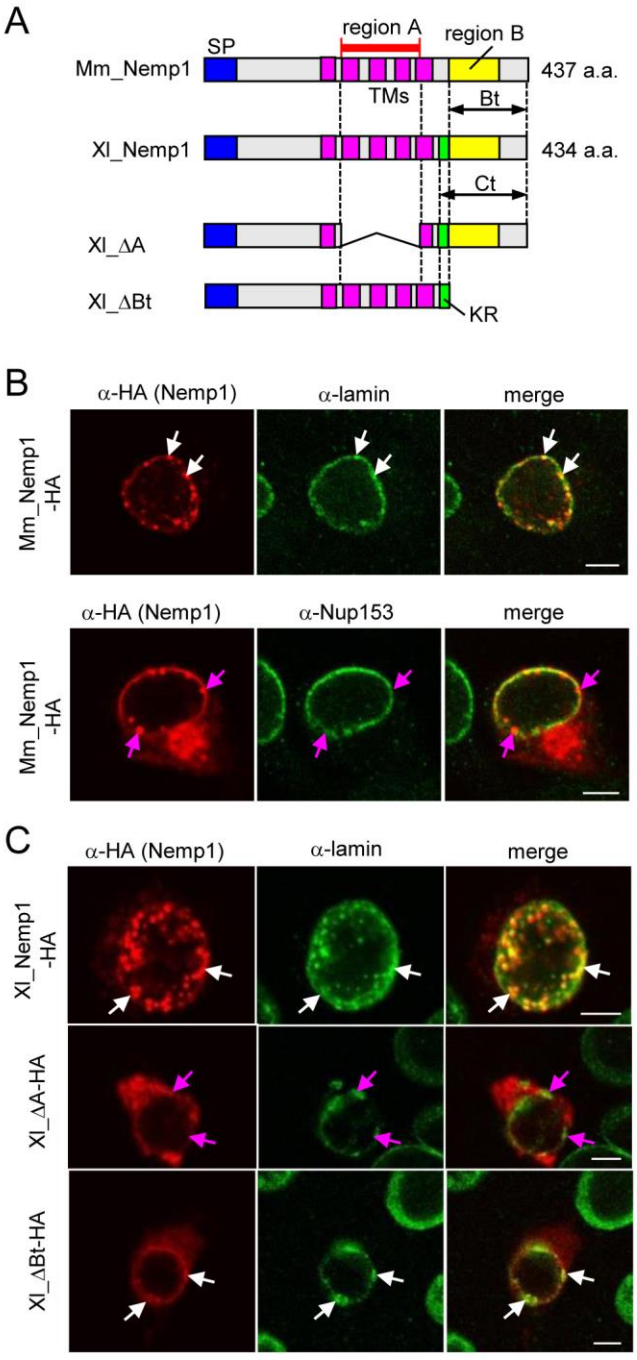
A
region A
region B
SP
Mm_Nemp1
437 a.a.
TMs
Bt
Xl_Nemp1
434 a.a.
Ct
Xl_ΔA
Xl_ΔBt
KR
B
α-HA (Nemp1)
α-lamin
merge
Mm_Nemp1 -HA
α-HA (Nemp1)
α-Nup153
merge
Mm_Nemp1 -HA
C
α-HA (Nemp1)
α-lamin
merge
Xl_Nemp1 -HA
Xl_ΔA-HA
Xl_ΔBt-HA

Figure 5

Figure 5 Colocalization of Nemp1 and lamins through region A

(A) The diagram of Xl_Nemp1 and Mm_Nemp1. Xl_Nemp1 but not Mm_Nemp1 contains the KR sequence. Blue, signal peptides (SP); magenta transmembrane domains (TMs); green, KR sequence; yellow boxes, region B. a.a., amino acid residues.

(B,C) Confocal analysis was performed using transfected COS-7 cells. (B) Mm_Nemp1-HA with lamin or Nup153. Transfected cells were stained with anti-HA (red) and anti-lamin or anti-Nup153 (green) antibody. Scale bars, 5 μm. (C) Xl_Nemp1-HA or its deletion mutants with lamin. Transfected cells were stained with anti-HA (red) and anti-lamin (green) antibodies. Scale bars, 5 μm.

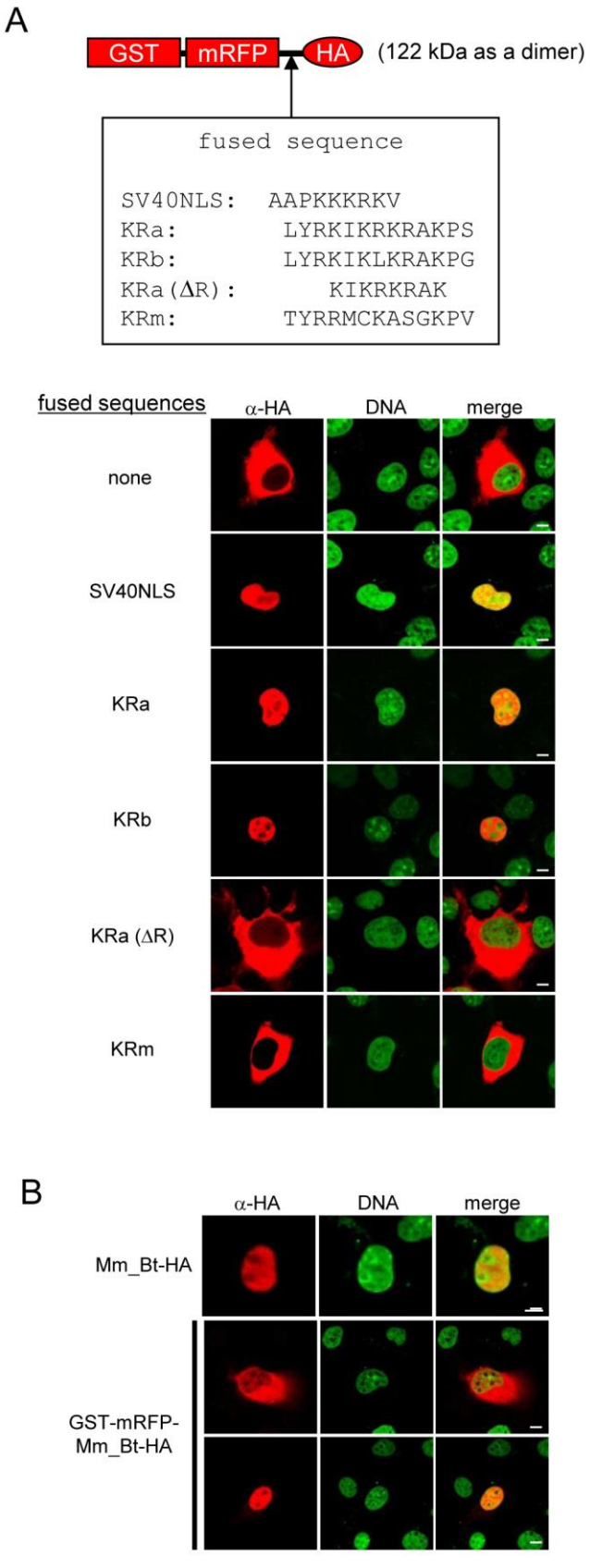
A
GST
mRFP
HA
(122 kDa as a dimer)
fused sequence
SV40NLS: AAPKKKRKV
KRa: LYRKIKRKRAKPS
KRb: LYRKIKLKRAKPG
KRa(ΔR): KIKRKRAK
KRm: TYRRMCKASGKPV
fused sequences
α-HA
DNA
merge
none
SV40NLS
KRa
KRb
KRa (ΔR)
KRm
B
α-HA
DNA
merge
Mm_Bt-HA
GST-mRFP-
Mm_Bt-HA

Figure 6

Figure 6 NLS function of the *Xenopus* KR sequence and Mm_Bt

(A) Subcellular localization of GST-mRFP fusion constructs for the *Xenopus* KR sequence. Upper panel, schematic representation of GST-mRFP fusion constructs. KRa, KRb, and KRm were derived from the KR of Xl_Nemp1a, Xl_Nemp1b, and the corresponding region of Mm_Nemp1, respectively. KRa(ΔR) is a deletion mutant of KRa. Lower panels, subcellular localization of GST-mRFP fusion constructs. COS-7 cells were transfected with HA-tagged GST-mRFP fusion constructs as indicated, fixed, and stained with anti-HA antibody (red) and SYTOX Green for DNA. Scale bars, 5 μm.

(B) Subcellular localization of Mm_Bt and its GST-mRFP- HA construct. COS-7 cells were transfected with the HA-tagged mouse Bt construct (Mm_Bt-HA) or GST-mRFP-Mm_Bt-HA, fixed, and stained with anti-HA antibody (red) and SYTOX Green for DNA. GST-mRFP-Mm_Bt-HA exhibited cytoplasmic localization (upper panels), but also nuclear localization in some cases (lower panels). Scale bars, 5 μm.

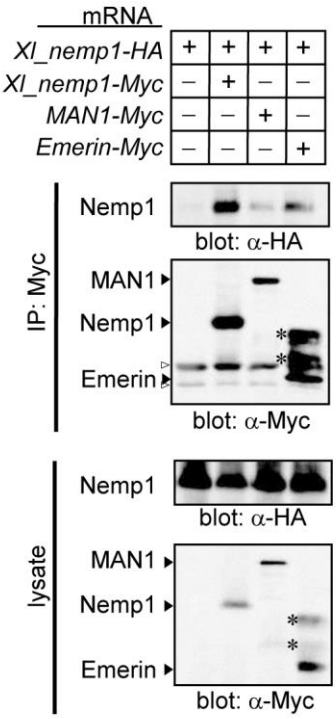

Figure 7 Interactions of Xl_Nemp1 with Xl_Nemp1 itself, MAN1, or Emerin

Co-IP of *Xl_Nemp1-HA* mRNA was coinjected into the animal pole region of two cell-stage *Xenopus* embryos with mRNA for *Xl_Nemp1-Myc*, *XMAN1-Myc*, or *Hs_emerin-Myc*. Injected embryos were collected at the late blastula stage (stage 9) and lysed with lysis buffer A. Black arrowheads, expected product bands; white arrowheads, immunoglobulin bands; asterisks, shifted bands of Emerin due to phosphorylation (Ellis et al., 1998).

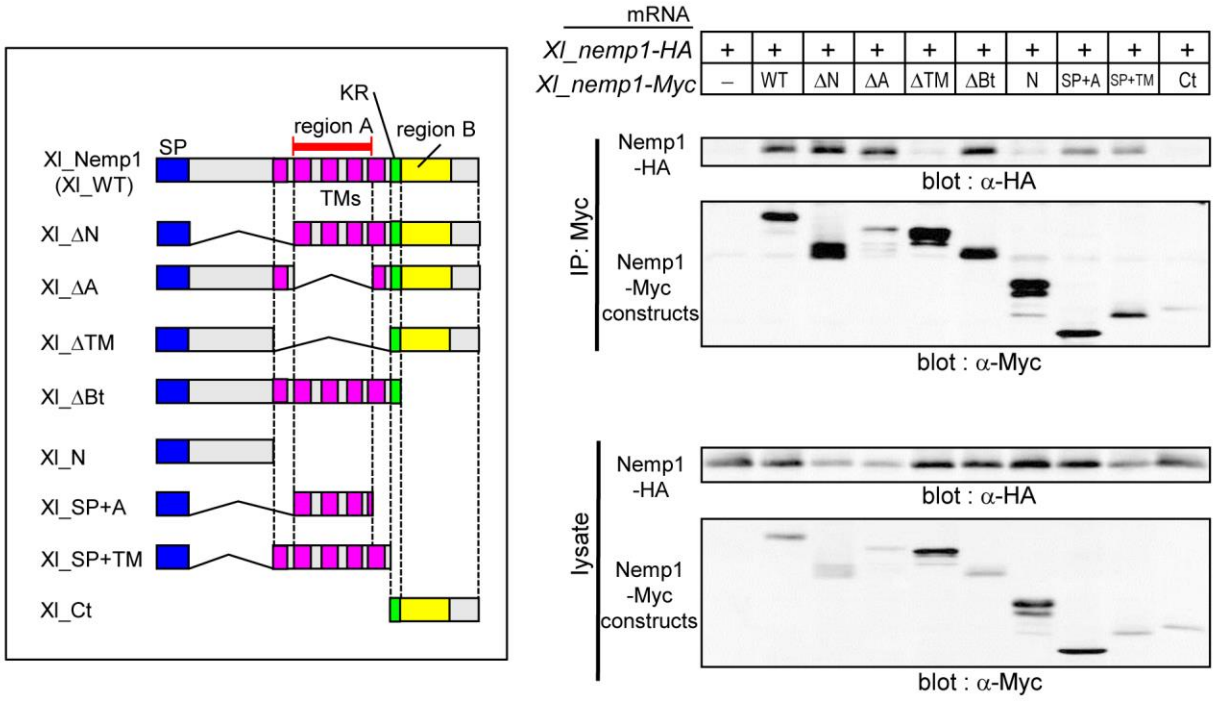

Figure 8 Oligomerization of Nemp1 through the TMs

Left panel, schematic structures of deletion constructs of Xl_Nemp1. Right Panel,. Co-IP of Nemp1 with its deletion constructs. mRNA for *Xl_Nemp1-HA* was injected into *Xenopus* embryos with mRNA for deletion constructs of *Xl_Nemp1-Myc*. After immunoprecipitation against Myc, western blotting was performed with anti-Myc or -HA antibody as indicated below each panel. WT, full length of Nemp1. Experimental conditions were the same as in Figure 7.

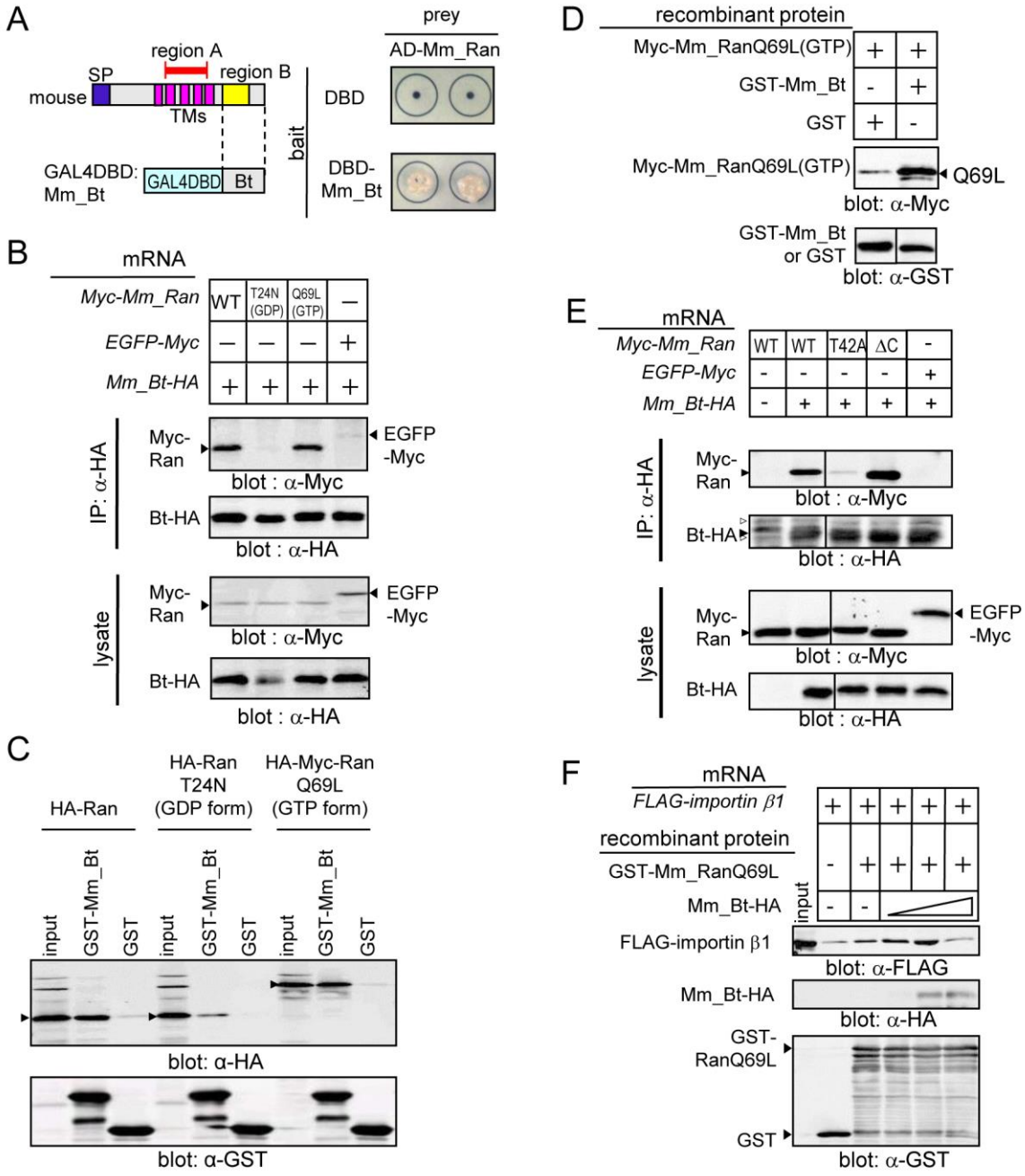

Figure 9 Interaction of region B with RanGTP

(A) Yeast two hybrid screening. Left panel, schematic representation of the bait, the Bt region of Mm_Nemp1 (DBD-Mm_Bt). Blue, signal peptides (SP); magenta transmembrane domains

(TMs); yellow boxes, region B. Right panels, colony formation (in duplicate) of yeast AH109 cells transformed with DBD (upper) or DBD-Mm_Bt (lower) with AD-Mm_Ran on plates lacking tryptophan, leucine, and adenine. DBD, the DNA binding domain of Gal4; AD, the activation domain of Gal4.

(B) Co-IP of region B with Ran or its mutants using *Xenopus* embryos. mRNA for *Mm_Bt-HA* was coinjected into *Xenopus* embryos with mRNA for *Myc-Mm_Ran*, the RanGDP form mutant *T24N*, the RanGTP form mutant *Q69L*, or *EGFP*. Experimental conditions were the same as in Figure 7.

(C) GST pulldown assays using *Xenopus* embryo lysates. Purified GST or GST-Mm_Bt protein absorbed onto glutathione-Sepharose beads were incubated with lysates of *Xenopus* embryos, which had been injected with mRNA for *HA-Mm_Ran*, *HA-T24N*, or *HA-Myc-Q69L* (500 pg/embryo). Proteins bound to the beads were analyzed by western blotting.

(D) In vitro binding assays with recombinant proteins, Myc-Mm_RanQ69L(GTP) and GST-Mm_Bt. Purified GST-Mm_Bt or GST (2.8 μg) was incubated with purified Myc-RanQ69L (5 μg), which had been loaded with 2 mM GTP in the binding buffer.

(E) Co-IP of Mm_Ran mutants T42A and ΔC with Mm_Bt-HA using *Xenopus* embryos. mRNA for *Mm_Bt-HA* was coinjected into *Xenopus* embryos with mRNA for *Myc-Mm_Ran*, or its mutants (*T42A* or *ΔC*). Experimental conditions were the same as in Figure 7. Unnecessary lanes were removed from a single blot.

(F) GST pulldown assays of GST-Mm_RanQ69L, importin β1 and Mm_Bt. *Xenopus* embryos were injected with mRNA for *FLAG-importin β1*. Lysates were added with 0.1, 1, 10 μg of recombinant Mm_Bt and glutathione beads absorbed 10 μg of GST-RanQ69L. Western blotting was performed with antibodies as indicated below each panel. Arrowheads, expected product bands. Proteins bound to the beads were analyzed by western blotting.

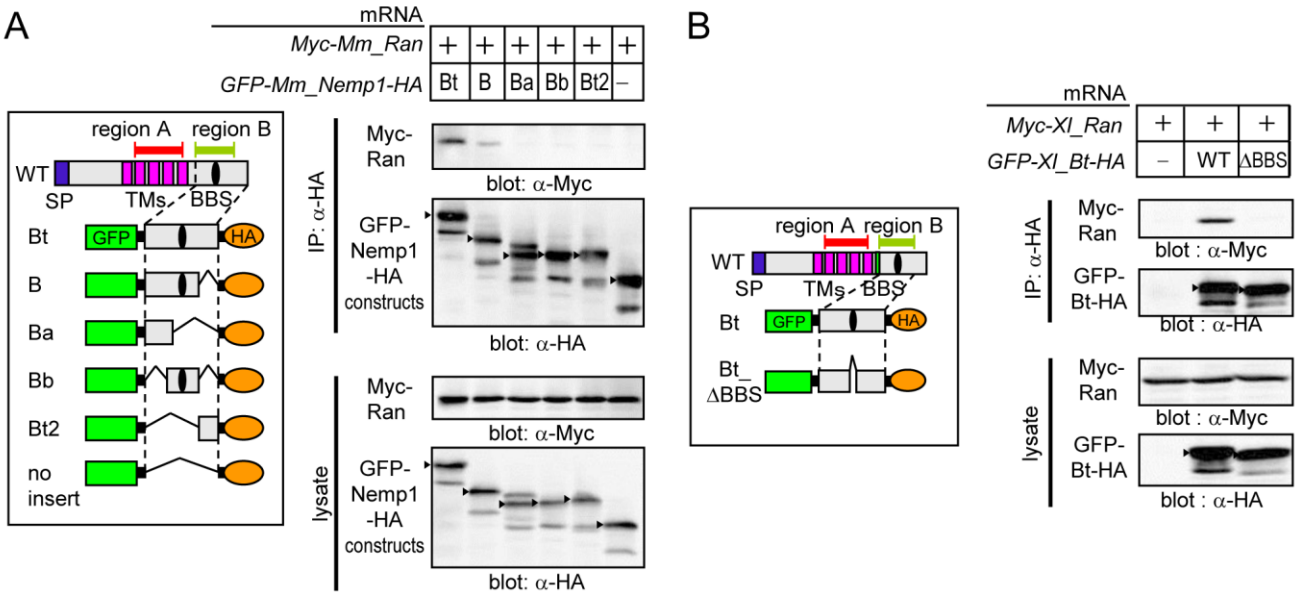

Figure 10 The binding region of region B for Ran

(A) Co-IP of Mm_Ran with deletion constructs of Mm_Bt. Left panel, schematic structures of Mm_Bt deletion constructs. Right panels, western blotting of immunoprecipitated proteins or lysates as indicated. mRNA for *Mm_Bt-HA* constructs was injected with mRNA for *Myc-Mm_Ran* into *Xenopus* embryos. Arrowheads, expected bands.

(B) Co-IP of Xl_Ran with Xl_Bt or Xl_Bt_ΔBBS. Left panel, schematic structures of Xl_Bt and Xl_Bt_ΔBBS constructs. Right panels, western blotting of immunoprecipitated proteins or lysates as indicated. Experimental conditions (A, B) were the same as in Figure 7.

Blue, signal peptides (SP); magenta transmembrane domains (TMs); green, GFP; black ovals, BBS.

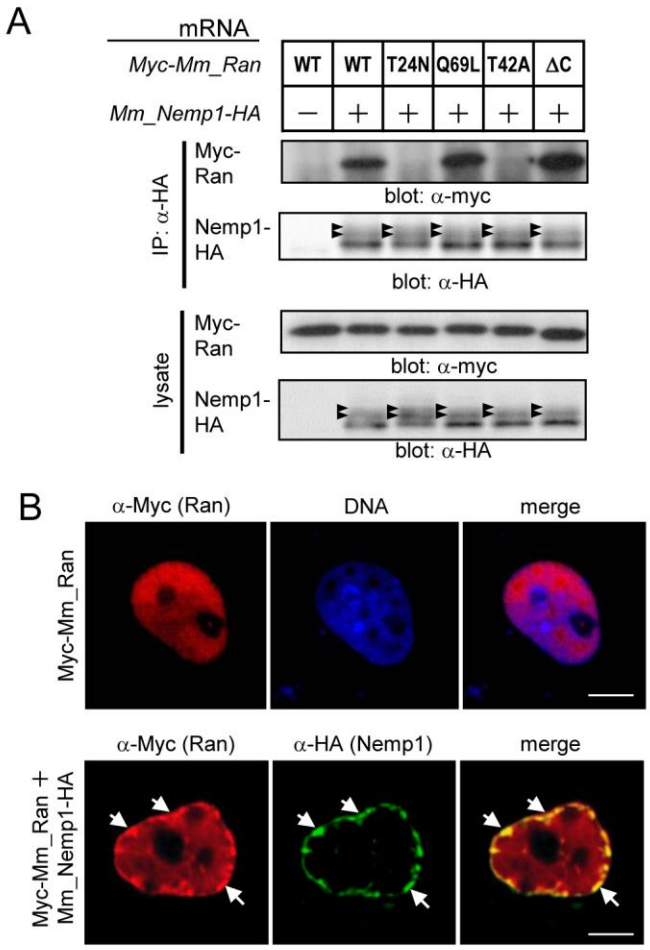

Figure 11 Interaction of Nemp1 with Ran at the NE

(A) Co-IP of Nemp1 with Ran or its mutants using *Xenopus* embryos. mRNA for *Mm_Nemp1-HA* was coinjected into *Xenopus* embryos with mRNA for *Myc-Mm_Ran* or its mutants (*T24N*, *Q69L*, *T42A*, *ΔC*). Injected embryos were collected at the mid blastula stage (stage 9) and lysed with lysis buffer B. Black arrowheads, modified forms of Nemp1. This data is the same as lanes 1-6 shown in Supplementary Figure 1. (B) Colocalization of Ran with Nemp1 at the nuclear periphery. COS-7 cells were transfected with Myc-Mm_Ran (red) with or without Mm_Nemp1-HA (green), and analyzed by confocal analysis. DNA was counterstained with SytoxGreen (blue). Scale bars, 5 μm.

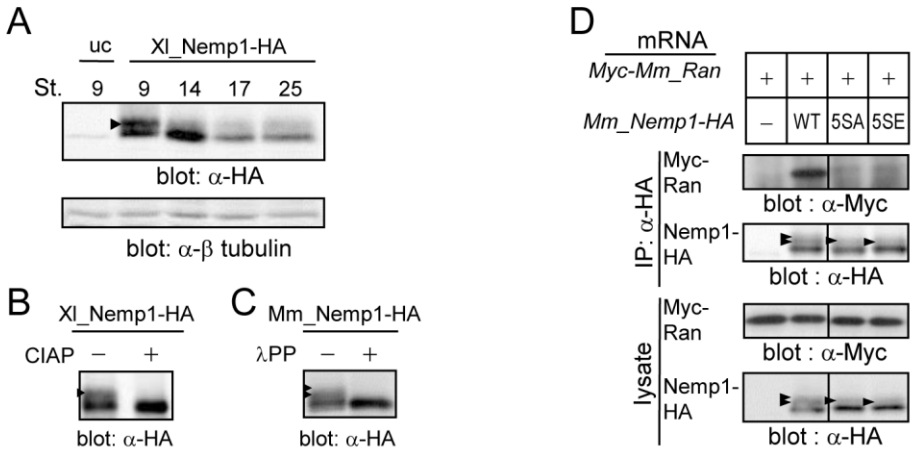

Figure 12 Phosphorylation of Nemp1

(A) Developmental analysis for modified Xl_Nemp1. *Xenopus* embryos were injected with mRNA for *Xl_Nemp1-HA* and collected at the indicated stages (St.). Lysates were subjected to western blotting with anti-HA or β tubulin antibody (loading control). uc, uninjected control.

(B) In vitro alkaline phosphatase assay of Xl_Nemp1. Lysates were prepared at the late blastula stage (stage 9). Xl_Nemp1-HA was immunoprecipitated by anti-HA antibody and treated with (+) or without (-) calf intestinal alkaline phosphatase (CIAP).

(C) In vitro alkaline phosphatase assay of Mm_Nemp1. Lysates were prepared at the mid blastula stage (stages 8-8.5), and treated with (+) or without (-) λ protein phosphatase (λPP).

(D) Co-IP of Mm_Ran with phosphorylation site mutants of Mm_Nemp1. mRNA for *Myc-Mm_Ran* was injected into *Xenopus* embryos with mRNA for *Mm_Nemp1-HA*, its alanine mutant (*5SA*), or its glutamic acid mutant (*5SE*). Injected embryos were collected at the mid blastula stage and lysed with lysis buffer B. This data is the same as lanes 1, 2, 7, and 8 shown in Supplementary Figure 1. Black arrowheads, modified forms.

A

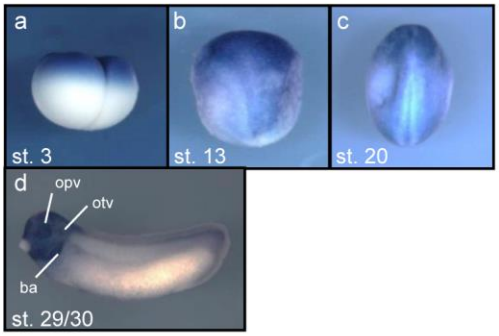

B

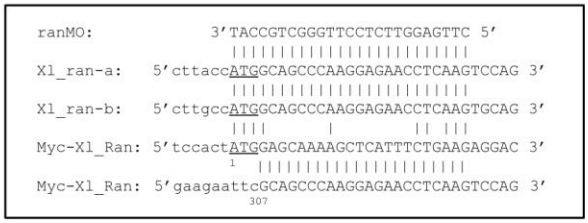

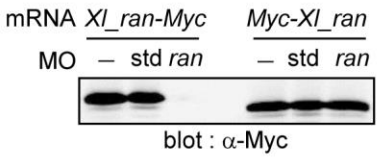

C

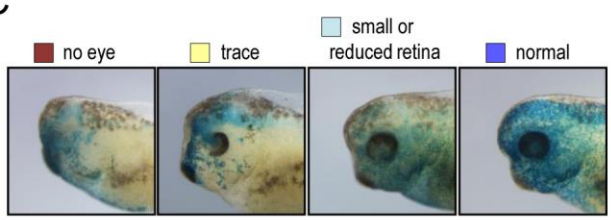

*nemp1*MOs (ng)	*ran*MO (ng)	stdMO (ng)
	10	
5		10
5	10	
10		10
10	10	
20		10
20	10	

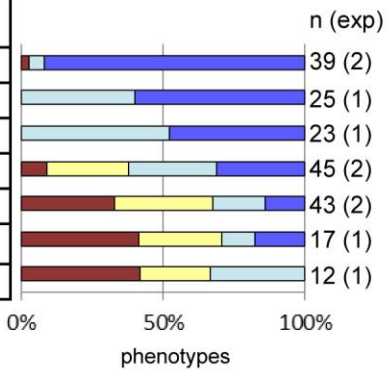

Figure 13

Figure 13 Cooperativity of Nemp1 and Ran in early eye development

(A) Spatiotemporal expression of *Xenopus ran* in the early development. Developmental stages are indicated. (a) Lateral view. (b, c) Dorsal view with the anterior side up. (d) Lateral view with the dorsal side up. opv, optic vesicles; otv, otic vesicles; ba, branchial arches.

(B) Specificity of *ran*MO. Nucleotide sequences of *Xl_ran-a* and *-b* mRNAs around the initiation codon (underlined), and *ran*MO (upper panel). Western blot analysis of Myc-tagged Xl_Ran fusion protein (lower panel). *ran*MO or stdMO (60 ng) was injected into both blastomeres of two cell stage embryos, and followed by injection with either 200 pg of *Xl_Ran-Myc* or *Myc-Xl_Ran* mRNA. –, embryos injected with mRNA alone.

(C) Eye defect phenotypes by knockdown of *nemp1* and *ran*. *nemp1*MOs (5-20 ng) and *nβ–gal* mRNA as a tracer (blue) were injected into the animal pole region of a dorsal blastomere at the four cell stage with *ran*MO or standard control MO (stdMO). Upper panels show eye-defect phenotypes at the tailbud stage (around stage 35) as indicated. The lower bar graph shows percentages of eye defects at tailbud stages. n, the number of embryos examined; exp, the number of independent experiments.

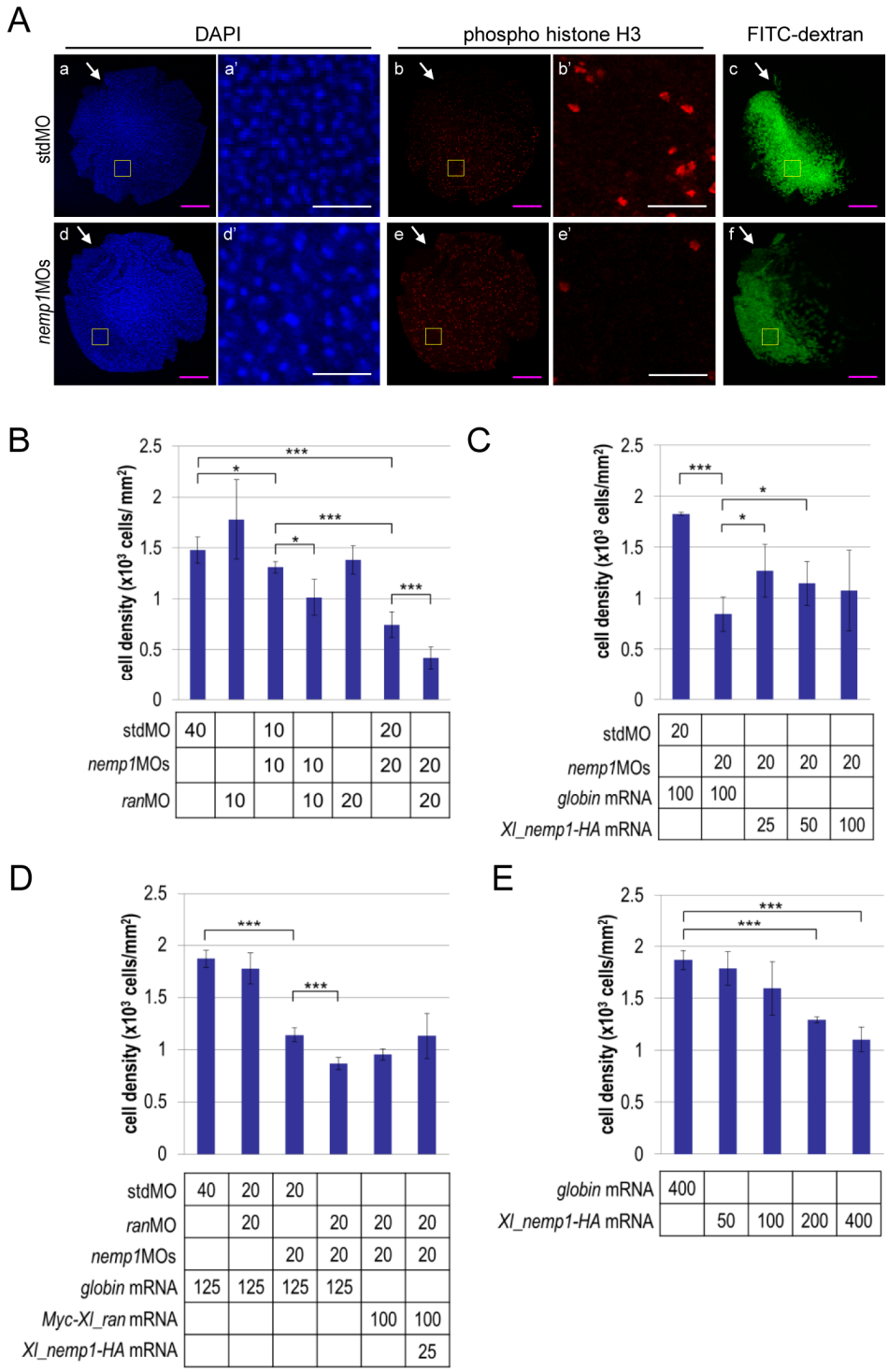
A
DAPI
phospho histone H3
FITC-dextran
stdMO
nemp1MOs
a
a'
b
b'
c
d
d'
e
e'
f
B
cell density (x10³ cells/ mm²)
stdMO 40 10 20
nemp1MOs 10 10 20 20
ranMO 10 10 20 20
C
cell density (x10³ cells/mm²)
stdMO 20
nemp1MOs 20 20 20 20
globin mRNA 100 100
Xl_nemp1-HA mRNA 25 50 100
D
cell density (x10³ cells/mm²)
stdMO 40 20 20
ranMO 20 20 20 20
nemp1MOs 20 20 20 20
globin mRNA 125 125 125 125
Myc-Xl_ran mRNA 100 100
Xl_nemp1-HA mRNA 25
E
cell density (x10³ cells/mm²)
globin mRNA 400
Xl_nemp1-HA mRNA 50 100 200 400

Figure 14

Figure 14 Reduction of cell densities by co-knockdown of *nemp1* and *ran*

(A) Effects of *nemp1*MOs on cell densities. Dorsoanterior views (a, b, c, d, e, f) of embryos are shown. Yellow boxes in a, b, d, and e correspond to enlarged areas a', b', d', and e', respectively. Upper panels, stdMO (40 ng/embryo); lower panels, *nemp1*MOs and stdMO (20 ng each/embryo) (the same experiment as in panel B). Embryos were injected with MOs and FITC-dextran as a tracer, fixed at stages 12.5-13, and immunostained with anti-phospho histone H3 antibody (red). DAPI was used for nuclear staining. White arrowheads, positions of blastopores; magenta scale bars, 500 μm; white scale bars, 100 μm.

(B) Synergistic effects of *nemp1*MOs and *ran*MO on cell densities. Combinations of MOs and amounts (ng/embryo) are as indicated. Experiments were repeated three times and similar results were obtained, one of which is presented here. DAPI-stained nuclei were counted in FITC-positive areas.

(C,D) Rescue of reduced cell density in morphants by mRNA injection. Combinations of MOs and mRNAs as well as amounts of MO (ng/embryo) and mRNA (pg/embryo) are as indicated. Injected embryos were fixed and immunostained using anti–HA antibody. DAPI-stained nuclei were counted in EGFP-HA positive areas.

(E) Reduction of cell densities by overexpression of Nemp1. Injected mRNA and amount (pg/embryo) are as indicated. DAPI-stained nuclei were counted in EGFP-HA positive areas.

*, $P<0.05$; ***, $P<0.005$; error bars, standard deviation.

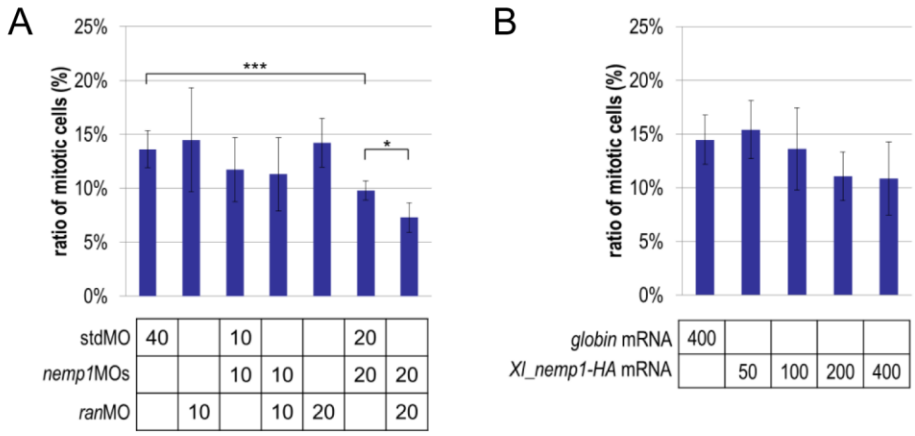

Figure 15 Gain- and loss-of-function experiments for the ratio of mitotic cells

Combinations of injected MOs and mRNAs as well as amounts of MO (ng/embryo) and mRNA (pg/embryo) are as indicated. Experiment conditions are the same as in Fig. 14.

(A) Reduction of the ratio of mitotic cells by co-knockdown of Nemp1 and Ran. Similar tendencies were obtained from the three experiments and statistically significant differences were observed in one of them. Nuclei stained with DAPI or immunostained for phospho histone H3 were counted in FITC-positive areas.

(B) Reduction of the ratio of mitotic cells by overexpression of Nemp1. DAPI-stained nuclei were counted in EGFP-HA positive areas.

*, $P<0.05$; ***, $P<0.005$; error bars, standard deviation.

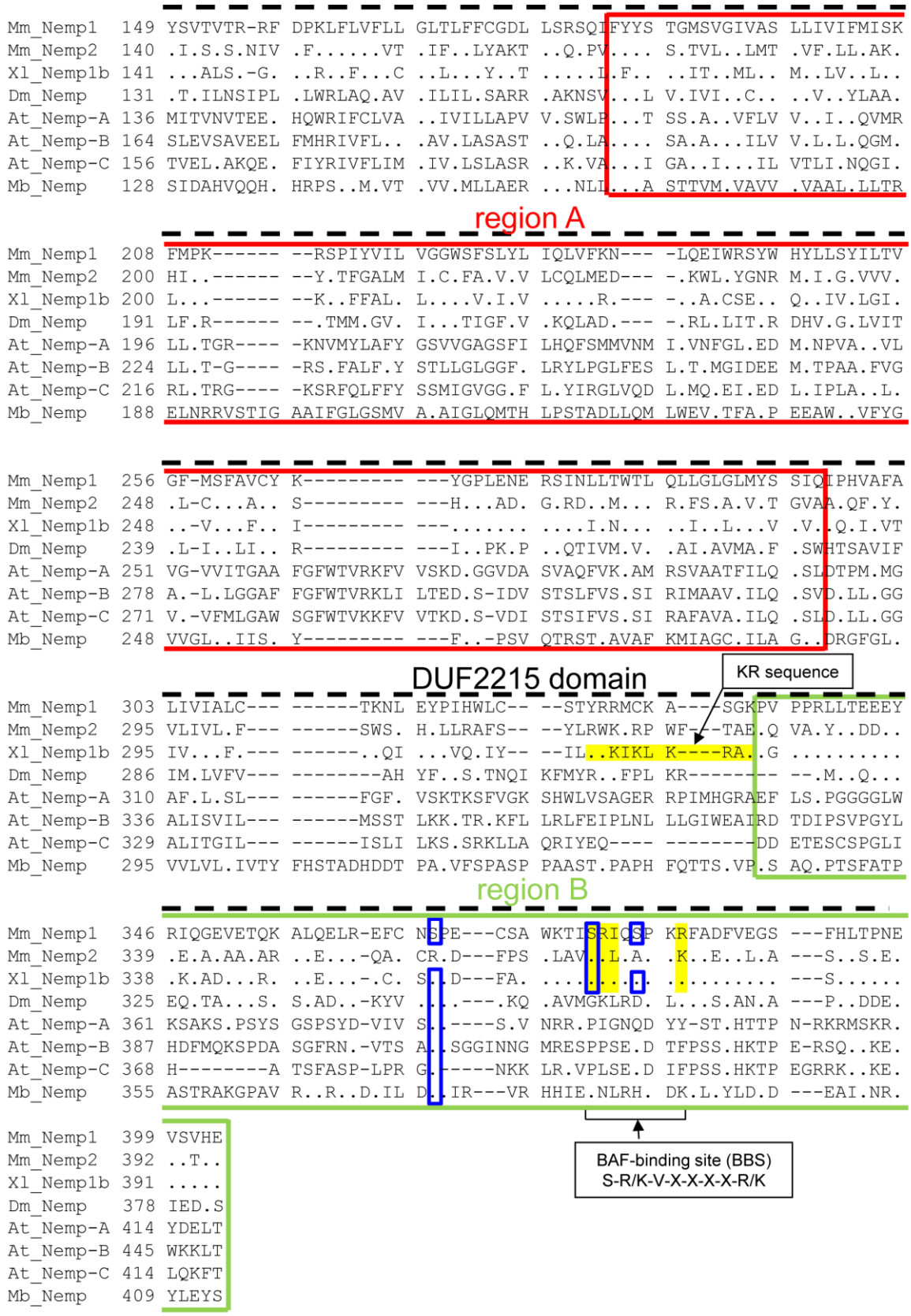
region A
DUF2215 domain
KR sequence
region B
BAF-binding site (BBS)
S-R/K-V-X-X-X-X-R/K

Figure 16

Figure 16 Amino acid sequence alignment of Nemp proteins

Only region A (red box) and region B (green box) were aligned for Mm_Nemp1, Mm_Nemp2, Xl_Nemp1b, Dm_Nemp, At_Nemp-A, At_Nemp-B, At_Nemp-C, and Mb_Nemp. Dots, identical amino acid residues; hyphens, gaps; dashed line, DUF2215 domain. The KR sequence and BAF binding sites are colored in yellow as indicated. Blue boxes indicates phosphorylation sites in Mm_Nemp1 and the corresponding serine residues in other species. The serine residues corresponding to Ser-366, Ser-376, and Ser380 (but not Ser419, and Ser420) in Mm_Nemp1 are conserved in Xl_Nemp1. BAF binding sites containing Ser380 are conserved in vertebrate Nemp1 and Nemp2, but not in others. At, *Arabidopsis thaliana*; Dm, *Drosophila melanogaster*; Mb, *Monosiga brevicollis* (choanoflagellate); Mm, *Mus musculus*; Xl, *Xenopus laevis*.

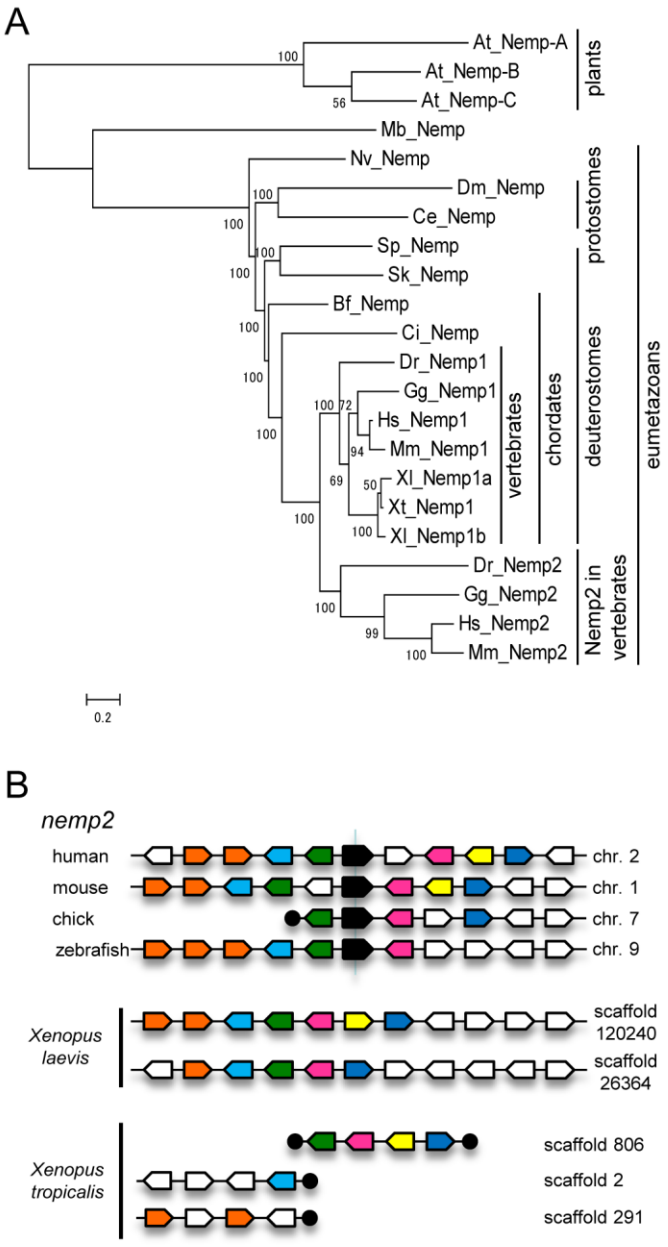
A
At_Nemp-A
At_Nemp-B
At_Nemp-C
plants
Mb_Nemp
Nv_Nemp
Dm_Nemp
Ce_Nemp
protostomes
Sp_Nemp
Sk_Nemp
Bf_Nemp
Ci_Nemp
Dr_Nemp1
Gg_Nemp1
Hs_Nemp1
Mm_Nemp1
Xl_Nemp1a
Xt_Nemp1
Xl_Nemp1b
vertebrates
chordates
deuterostomes
eumetazoans
Dr_Nemp2
Gg_Nemp2
Hs_Nemp2
Mm_Nemp2
Nemp2 in vertebrates
0.2
B
nemp2
human
mouse
chick
zebrafish
chr. 2
chr. 1
chr. 7
chr. 9
Xenopus laevis
scaffold 120240
scaffold 26364
Xenopus tropicalis
scaffold 806
scaffold 2
scaffold 291

Figure 17

Figure 17 Phylogenetic and syntenic analyses of the Nemp family

(A) Phylogenetic analysis. A phylogenetic tree was constructed by the Maximum Likelihood (ML) method using Treefinder with the protein matrix LG after amino acid sequences of the DUF2215 domain in various organisms were aligned using the ClustalW alignment tool with the Gonnet series protein weight matrix (see Fig. 16) and trimmed using trimAl. Values beside nodes show the number of times that a node was supported in 1000 bootstrap pseudoreplication. The scale bar represents a distance of 0.2 substitutions per site. *Arabidopsis* Nemp homologs (At_Nemp-A, B, and C) serve as outgroups. Note that Nemp is evolutionary conserved from metazoans to choanoflagellates to plants, mainly in the terminal part of region A (see Fig. 16). In vertebrates, a Nemp1 homolog, named TMEM194B or Nemp2, is present in the genome databases of zebrafish, chick, mice, and humans. A de novo phylogenetic tree revealed that Nemp1 and Nemp2 form sister groups in vertebrates (not shown), indicating that Nemp2 is the vertebrate paralog of Nemp1. Abbreviations of species and common names are as follows: plant *Arabidopsis thaliana* (At), Florida lancelet *Branchiostoma floridae* (Bf), nematode *Caenorhabditis elegans* (Ce), ascidian *Ciona intestinalis* (Ci), *Drosophila melanogaster* (Dm), zebrafish *Danio rerio* (Dr), chick *Gallus gallus* (Gg), human *Homo sapiens* (Hs), choanoflagellate *Monosiga brevicollis* (Mb), mouse *Mus musculus* (Mm), sea anemone *Nematostella vectensis* (Nv), *Saccoglossus kowalevskii* (Sk), *Strongylocentrotus purpuratus* (Sp), African clawed frog *Xenopus laevis* (Xl), and western clawed frog *Xenopus tropicalis* (Xt). Accession numbers of amino acid sequences: Hs_Nemp1, O14524; Mm_Nemp1, Q6ZQE4; Gg_Nemp1, XM_001232566; Xl_Nemp1a, NP_001090391; Xl_Nemp1b, NP_001091224; Xt_Nemp1, NP_001034832; Dr_Nemp1, XP_683418; Hs_Nemp2, A6NFY4; Mm_Nemp2, Q8CB65; Gg_Nemp2, Q5ZJY9; Dr_Nemp2, XP_693037; Bf_Nemp, XP_002585718; Ci_Nemp, AK116477; Sk_Nemp, XP_002741981; Sp_Nemp, XP_001196379; Dm_Nemp, NP_573142; Ce_Nemp, NP_497202; Nv_Nemp, XP_001640959; At_Nemp-A, NM_102639; At_Nemp-B, NM_001037091; At_Nemp-C, NM_114844;

Mb_Nemp, XP_001742508.

(B) Conserved synteny of vertebrate *nemp2* genes. A boat-shape object represents a gene with a direction, in which the tip of boat corresponds to the 3' end of the gene. Genes indicated with a same color mean orthologous genes, in which white boats indicates unrelated genes. Black boats indicate *nemp2*. Black circles indicate the ends of chromosomes or scaffolds. These maps are drawn based on JGI Metazome data, with some manual editing and corrections. The corresponding synteny maps of *X. laevis* (ver. 7.1) and *X. tropicalis* (ver. 7.1) suggest that *Xenopus* species do not have *nemp2* orthologs. In addition, EST databases for *X. laevis* and *X. tropicalis* do not contain *nemp2*-like sequences.

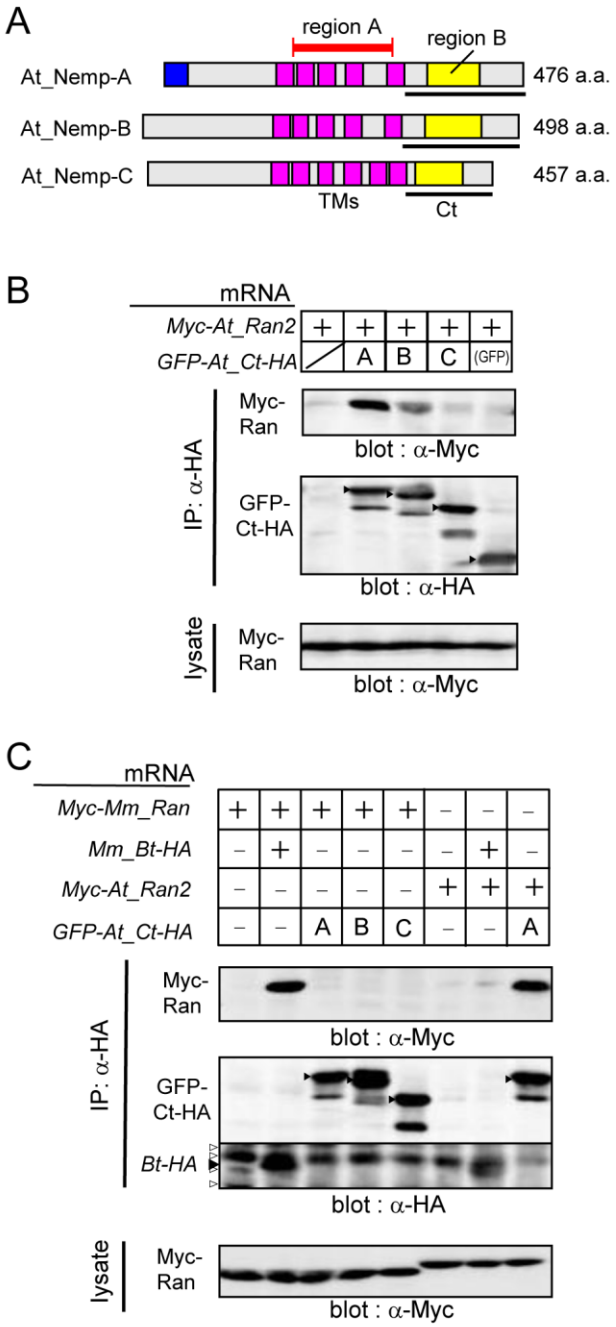
A
region A
region B
At_Nemp-A
476 a.a.
At_Nemp-B
498 a.a.
At_Nemp-C
457 a.a.
TMs
Ct
B
mRNA
Myc-At_Ran2
GFP-At_Ct-HA
A
B
C
(GFP)
IP: α-HA
Myc-Ran
blot : α-Myc
GFP-Ct-HA
blot : α-HA
lysate
Myc-Ran
blot : α-Myc
C
mRNA
Myc-Mm_Ran
Mm_Bt-HA
Myc-At_Ran2
GFP-At_Ct-HA
IP: α-HA
Myc-Ran
blot : α-Myc
GFP-Ct-HA
Bt-HA
blot : α-HA
lysate
Myc-Ran
blot : α-Myc

Figure 18

Figure 18 Evolutionary conservation of Ran binding of region B in *Arabidopsis*

(A) Diagram of Arabidopsis Nemp-A, -B, and -C proteins. According to the Arabidopsis genome sequence, typical signal peptide (SP) sequences were not detected in At_Nemp-B and At_Nemp-C. At_Nemp-C is predicted to contain six TMs, but the last two TMs may be a single TM. Colored boxes: blue, signal peptides (SP); magenta, transmembrane domains (TMs); yellow, region B. a.a., amino acid residues.

(B) Co-IP of At_Nemp and At_Ran. Because region B of At_Nemp proteins are not well defined by comparison to vertebrate Nemp1, which is attributed to low amino acid conservation, the entire C-terminal regions downstream of the last TM (named Ct, see Fig. 18A) were used for co-IP experiments. mRNA for *GFP-At_Ct-HA* constructs were injected with mRNA for *Myc-At_Ran2* into *Xenopus* embryos.

(C) Co-IP of At_Nemp with Mm_Ran or Mm_Nemp1 with At_Ran2. *Xenopus* embryos were coinjected with combinations of mRNAs as indicated. Experimental conditions were the same as in Figure 7. Black arrowhead, expected product bands; white arrowheads, cross-reacted bands. After immunoprecipitation against HA, western blotting was performed with anti-Myc or HA antibody as indicated.

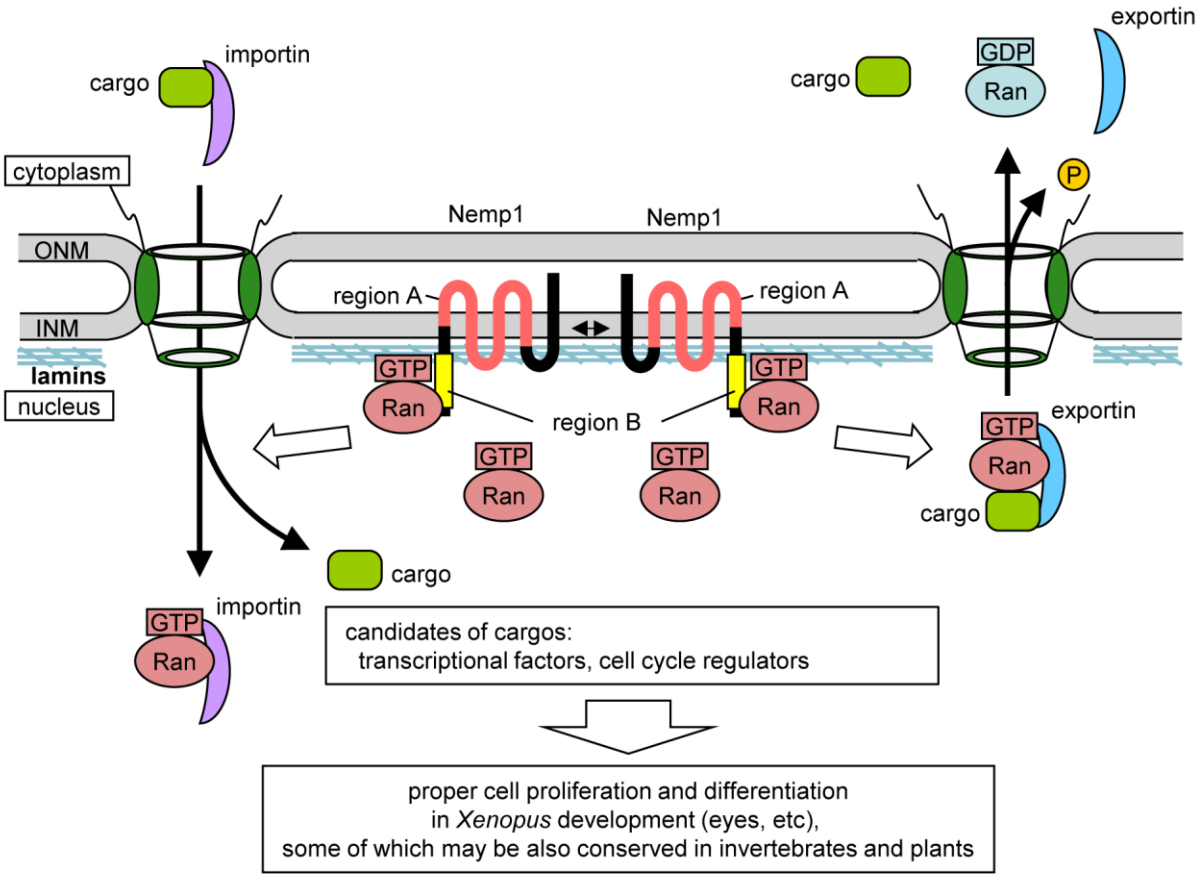

Figure 19 Proposed model of molecular functions of Nemp1.

Nemp1 forms a complex with Nemp1 itself at the INM. Nemp1 accumulate RanGTP near the INM through the binding of region B to RanGTP. Concentrated RanGTP may facilitate the nuclear transport of various factors, some of which are associated with cell proliferation and differentiation.

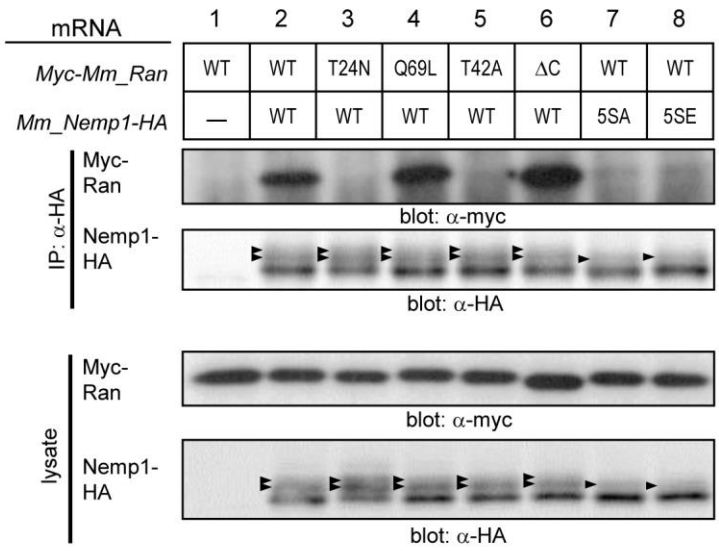

Supplemental figure 1 Co-IP of Nemp1 with Ran using *Xenopus* embryos

This is the original data for Figures 11A and 12D. mRNA for *Mm_Nemp1-HA* or its mutants (*5SA*, *5SE*) was coinjected into *Xenopus* embryos with mRNA for *Myc-Mm_Ran* (WT) or its mutants (*T24N*, *Q69L*, *T42A*, *ΔC*). Injected embryos were collected at the mid blastula stage (stages 8-8.5) and lysed with lysis buffer B for Co-IP. Black arrowheads, modified forms of Nemp1-HA. Note that WT Nemp1 has two major modified bands (lane 2) and co-expression with Ran(T24N; a GDP form) enhanced these modifications (lane 3). Also note that the upper modified band disappeared in 5SA and 5SE constructs (lanes 7, 8), suggesting that all or some of these five serine residues are involved in modification (phosphorylation) by functioning as either phosphorylation sites or recognition sites or both, and that there are other phosphorylation sites besides there five serine residues.

References

Bamba, C., Bobinnec, Y., Fukuda, M., and Nishida, E. (2002). The GTPase Ran regulates chromosome positioning and nuclear envelope assembly in vivo. Curr Biol *12*, 503-507.

Bian, Y., Song, C., Cheng, K., Dong, M., Wang, F., Huang, J., Sun, D., Wang, L., Ye, M., and Zou, H. (2014). An enzyme assisted RP-RPLC approach for in-depth analysis of human liver phosphoproteome. J Proteomics *96*, 253-262.

Cautain, B., Hill, R., de Pedro, N., and Link, W. (2015). Components and regulation of nuclear transport processes. Febs J *282*, 445-462.

Chook, Y. M., and Blobel, G. (1999). Structure of the nuclear transport complex karyopherin-beta2-Ran x GppNHp. Nature *399*, 230-237.

Ciska, M., Masuda, K., and Moreno Diaz de la Espina, S. (2013). Lamin-like analogues in plants: the characterization of NMCP1 in Allium cepa. J Exp Bot *64*, 1553-1564.

Clarke, P. R., and Zhang, C. (2008). Spatial and temporal coordination of mitosis by Ran GTPase. Nat Rev Mol Cell Biol *9*, 464-477.

Daub, H., Olsen, J. V., Bairlein, M., Gnad, F., Oppermann, F. S., Korner, R., Greff, Z., Keri, G., Stemmann, O., and Mann, M. (2008). Kinase-selective enrichment enables quantitative phosphoproteomics of the kinome across the cell cycle. Mol Cell *31*, 438-448.

Dephoure, N., Zhou, C., Villen, J., Beausoleil, S. A., Bakalarski, C. E., Elledge, S. J., and Gygi, S. P. (2008). A quantitative atlas of mitotic phosphorylation. Proc Natl Acad Sci USA *105*, 10762-10767.

Dittmer, T. A., Stacey, N. J., Sugimoto-Shirasu, K., and Richards, E. J. (2007). LITTLE NUCLEI genes affecting nuclear morphology in Arabidopsis thaliana. Plant Cell *19*, 2793-2803.

Ellis, J. A., Craxton, M., Yates, J. R., and Kendrick-Jones, J. (1998). Aberrant intracellular targeting and cell cycle-dependent phosphorylation of emerin contribute to the Emery-Dreifuss muscular dystrophy phenotype. J Cell Sci *111 (Pt 6)*, 781-792.

Feldherr, C. M., and Akin, D. (1994). Variations in signal-mediated nuclear transport during the cell cycle in BALB/c 3T3 cells. Exp Cell Res *215*, 206-210.

Graumann, K., and Evans, D. E. (2010). Plant SUN domain proteins: components of putative plant LINC complexes? Plant Signal Behav *5*, 154-156.

Gruenbaum, Y., Margalit, A., Goldman, R. D., Shumaker, D. K., and Wilson, K. L. (2005). The nuclear lamina comes of age. Nat Rev Mol Cell Biol *6*, 21-31.

Hahn, S., and Schlenstedt, G. (2011). Importin beta-type nuclear transport receptors have distinct binding affinities for Ran-GTP. Biochem Biophys Res Commun *406*, 383-388.

Harland, R. M. (1991). In situ hybridization: an improved whole-mount method for Xenopus embryos. In Methods Cell Biol., B. K. Kay, and H. B. Peng, eds. (San Diego, CA, Academic Press), pp. 685-695.

Hiratani, I., Yamamoto, N., Mochizuki, T., Ohmori, S. Y., and Taira, M. (2003). Selective degradation of excess Ldb1 by Rnf12/RLIM confers proper Ldb1 expression levels and Xlim-1/Ldb1 stoichiometry in Xenopus organizer functions. Development *130*, 4161-4175.

Hocevar, B. A., Burns, D. J., and Fields, A. P. (1993). Identification of protein kinase C (PKC) phosphorylation sites on human lamin B. Potential role of PKC in nuclear lamina structural dynamics. J Biol Chem *268*, 7545-7552.

Huang, Y., Cai, M., Clore, G. M., and Craigie, R. (2011). No interaction of barrier-to-autointegration factor (BAF) with HIV-1 MA, cone-rod homeobox (Crx) or MAN1-C in absence of DNA. PLoS One *6*, e25123.

Hughes, M., Zhang, C., Avis, J. M., Hutchison, C. J., and Clarke, P. R. (1998). The role of the ran GTPase in nuclear assembly and DNA replication: characterisation of the effects of Ran mutants. J Cell Sci *111 (Pt 20)*, 3017-3026.

Kettenbach, A. N., Schweppe, D. K., Faherty, B. K., Pechenick, D., Pletnev, A. A., and Gerber, S. A. (2011). Quantitative phosphoproteomics identifies substrates and functional modules of Aurora and Polo-like kinase activities in mitotic cells. Sci Signal *4*, rs5.

King, M. C., Lusk, C. P., and Blobel, G. (2006). Karyopherin-mediated import of integral inner nuclear membrane proteins. Nature *442*, 1003-1007.

Li, S., Armstrong, C. M., Bertin, N., Ge, H., Milstein, S., Boxem, M., Vidalain, P. O., Han, J. D., Chesneau, A., Hao, T., *et al.* (2004). A map of the interactome network of the metazoan C. elegans. Science *303*, 540-543.

Ma, L., Hong, Z., and Zhang, Z. (2007). Perinuclear and nuclear envelope localizations of Arabidopsis Ran proteins. Plant Cell Rep *26*, 1373-1382.

Mamada, H., Takahashi, N., and Taira, M. (2009). Involvement of an inner nuclear membrane protein, Nemp1, in Xenopus neural development through an interaction with the chromatin protein BAF. Dev Biol *327*, 497-507.

Mans, B. J., Anantharaman, V., Aravind, L., and Koonin, E. V. (2004). Comparative genomics, evolution and origins of the nuclear envelope and nuclear pore complex. Cell Cycle *3*, 1612-1637.

Mansharamani, M., and Wilson, K. L. (2005). Direct binding of nuclear membrane protein MAN1 to emerin in vitro and two modes of binding to barrier-to-autointegration factor. J Biol Chem *280*, 13863-13870.

Markiewicz, E., Tilgner, K., Barker, N., van de Wetering, M., Clevers, H., Dorobek, M., Hausmanowa-Petrusewicz, I., Ramaekers, F. C., Broers, J. L., Blankesteijn, W. M., *et al.* (2006). The inner nuclear membrane protein emerin regulates beta-catenin activity by restricting its accumulation in the nucleus. Embo J *25*, 3275-3285.

Merkle, T. (2011). Nucleo-cytoplasmic transport of proteins and RNA in plants. Plant Cell Rep *30*, 153-176.

Mii, Y., and Taira, M. (2009). Secreted Frizzled-related proteins enhance the diffusion of Wnt ligands and expand their signalling range. Development *136*, 4083-4088.

Murphy, G. A., Moore, M. S., Drivas, G., Perez de la Ossa, P., Villamarin, A., D'Eustachio, P., and Rush, M. G. (1997). A T42A Ran mutation: differential interactions with effectors and

regulators, and defect in nuclear protein import. Mol Biol Cell *8*, 2591-2604.

Nieuwkoop, P. D., and Faber, J. (1967). Normal Table of Xenopus laevis (Daudin) (Amsterdam, North Holland).

Olins, A. L., Rhodes, G., Welch, D. B., Zwerger, M., and Olins, D. E. (2010). Lamin B receptor: multi-tasking at the nuclear envelope. Nucleus *1*, 53-70.

Onuma, Y., Nishihara, R., Takahashi, S., Tanegashima, K., Fukui, A., and Asashima, M. (2000). Expression of the Xenopus GTP-binding protein gene Ran during embryogenesis. Dev Genes Evol *210*, 325-327.

Osada, S., Ohmori, S. Y., and Taira, M. (2003). XMAN1, an inner nuclear membrane protein, antagonizes BMP signaling by interacting with Smad1 in Xenopus embryos. Development *130*, 1783-1794.

Peter, A., and Reimer, S. (2012). Evolution of the lamin protein family: what introns can tell. Nucleus *3*, 44-59.

Peter, M., Nakagawa, J., Doree, M., Labbe, J. C., and Nigg, E. A. (1990). In vitro disassembly of the nuclear lamina and M phase-specific phosphorylation of lamins by cdc2 kinase. Cell *61*, 591-602.

Ploski, J. E., Shamsher, M. K., and Radu, A. (2004). Paired-type homeodomain transcription factors are imported into the nucleus by karyopherin 13. Mol Cell Biol *24*, 4824-4834.

Razafsky, D., and Hodzic, D. (2009). Bringing KASH under the SUN: the many faces of nucleo-cytoskeletal connections. J Cell Biol *186*, 461-472.

Sakamoto, Y., and Takagi, S. (2013). LITTLE NUCLEI 1 and 4 regulate nuclear morphology in Arabidopsis thaliana. Plant Cell Physiol *54*, 622-633.

Schirmer, E. C., Florens, L., Guan, T., Yates, J. R., 3rd, and Gerace, L. (2003). Nuclear membrane proteins with potential disease links found by subtractive proteomics. Science *301*, 1380-1382.

Sharma, K., D'Souza, R. C., Tyanova, S., Schaab, C., Wisniewski, J. R., Cox, J., and Mann, M.

(2014). Ultradeep human phosphoproteome reveals a distinct regulatory nature of Tyr and Ser/Thr-based signaling. Cell Rep *8*, 1583-1594.

Shibano, T., Takeda, M., Suetake, I., Kawakami, K., Asashima, M., Tajima, S., and Taira, M. (2007). Recombinant Tol2 transposase with activity in Xenopus embryos. FEBS Lett *581*, 4333-4336.

Stewart, M. (2007). Molecular mechanism of the nuclear protein import cycle. Nat Rev Mol Cell Biol *8*, 195-208.

Tseng, L. C., and Chen, R. H. (2011). Temporal control of nuclear envelope assembly by phosphorylation of lamin B receptor. Mol Biol Cell *22*, 3306-3317.

Vernon, A. E., and Philpott, A. (2003). The developmental expression of cell cycle regulators in Xenopus laevis. Gene Expr Patterns *3*, 179-192.

Vetter, I. R., Nowak, C., Nishimoto, T., Kuhlmann, J., and Wittinghofer, A. (1999). Structure of a Ran-binding domain complexed with Ran bound to a GTP analogue: implications for nuclear transport. Nature *398*, 39-46.

Villa Braslavsky, C. I., Nowak, C., Gorlich, D., Wittinghofer, A., and Kuhlmann, J. (2000). Different structural and kinetic requirements for the interaction of Ran with the Ran-binding domains from RanBP2 and importin-beta. Biochemistry *39*, 11629-11639.

Wilson, K. L., and Berk, J. M. (2010). The nuclear envelope at a glance. J Cell Sci *123*, 1973-1978.

Wilson, K. L., and Dawson, S. C. (2011). Evolution: functional evolution of nuclear structure. J Cell Biol *195*, 171-181.

Wu, W., Lin, F., and Worman, H. J. (2002). Intracellular trafficking of MAN1, an integral protein of the nuclear envelope inner membrane. J Cell Sci *115*, 1361-1371.

Zuleger, N., Robson, M. I., and Schirmer, E. C. (2011). The nuclear envelope as a chromatin organizer. Nucleus *2*, 339-349.